Alluvial Fan Flood Hazard Assessment based on DTM Uncertainty

Tarick Hosein

February, 2010

Alluvial Fan Flood Hazard Assessment based on DTM Uncertainty

by

Tarick Hosein

Thesis submitted to the International Institute for Geo-information Science and Earth Observation in partial fulfilment of the requirements for the degree of Master of Science in Geo-information Science and Earth Observation, Specialisation: (Geo-Hazards)

Thesis Assessment Board

Chairman:	Prof.Dr. V.G. Jetten
External Examineer:	Dr. R. van Beek
First Supervisor:	Dr. M.W. Straatsma
Second Supervisor:	Dr. D. Alkema
Advisor:	Drs. T.M. Loran

INTERNATIONAL INSTITUTE FOR GEO-INFORMATION SCIENCE AND EARTH OBSERVATION
ENSCHEDE, THE NETHERLANDS

Disclaimer

This document describes work undertaken as part of a programme of study at the International Institute for Geo-information Science and Earth Observation. All views and opinions expressed therein remain the sole responsibility of the author, and do not necessarily represent those of the institute.

Abstract

Alluvial fan flooding is considered to be one of the most dangerous form of flooding. Its assessment is difficult because of unpredictable flow paths brought about by dynamic terrain changes, such as sediment disposition, that occur during an event. The aim of this study was to assess the influence of DTM uncertainty on flood patterns, particularly on concentrated impulse paths. In order to better understand the consequences of such a flood, the study included an investigation of storms as the event triggers, and debris infilling and blockage as processes. Terrain dynamics were studied in the form of spatially correlated and uncorrelated noise added to the DTM to understand the effect of DTM uncertainty. The results in storm designs reflected the difficulty associated with spatially varying weather systems within ungauged mountainous watersheds. Channel backfilling was found to require over 100000m3 of debris material before potentially placing the whole alluvial fan at risk of flooding. During such a flooding scenario, the study found that there are systematic and unsystematic runoff flow path responses. This was found to be dependent on the design of noise added to the DTM. The use of spatially correlated noise gave biased systematic flow paths in the flood model. However, the results of the uncorrelated noise reflects typical flow path expectations, during such flooding. The addition of noise to the DTM can give a useful insight of the consequences of flooding in general, however the model of noise added should reflect the processes that may cause uncertainty.

Keywords:
Alluvial Fan; Flooding; Flood Hazard Assessment ;Uncertainty; DTM

Acknowledgements

In the name of Allah most Generous most Merciful

Alhamdulillah lil rab el alamei, All praise is due to Allah, to whom I am most thankful for all he has given me and my family, and for the completion of this thesis.

This thesis would not have been possible without the assistance of the International Institute for Geo-Information science and Earth Observations (ITC) and United Nations University, who sponsored my studies.

I am heartily thankful to my supervisors, Dr. Menno Straatsma and Dr. Dinand Alkema, whose guidance and support facilitate my growth and understanding of the subject.

I am very much grateful to Professor Dr. Victor Jetten for his assistance in PcRaster and LISEM.

I am indebted to Drs. Nanette Kingma and Rob Hennemann for the coordination and field support given during data collection.

I would also like to show my gratitude to Byron Luna, Simone Frigerio, Marjory Angignard and Melanie Kappes, who greatly provided supported in data collection and information gathering.

It is an honour for me to thank the RTM services in Barcelonnette , Dr. Jean-Philippe Mallet, Dr. Alexandre Remaitre and the Mountain Risk Project Consortium for sharing their research data and knowledge of the Faucon study area and giving me the opportunity to be part of their ongoing research.

Finally, I would like to thank all staff and students at ITC for their support and encouragement throughout the last 18 months.

Tarick Hosein
February 2010
Enschede
The Netherlands

Table of contents

List of figures

List of tables

1. Introduction

1.1. Introduction

On the geological time scale, alluvial fans are dynamic landforms created by multiple processes, the most significant of which is flooding. Although the sloping landform reduces the risk of flood inundation, its surrounding geomorphologic environment increases the risk of a more serious form of flooding referred to as "alluvial fan flooding" (NRC 1996). Whereas flood hazards are defined in terms of inundation extent, velocity, depth, duration, arrival time of flood waters, alluvial fans have lower flood depths but higher flow velocities and arrival times. As a result of the high velocities and sediment rich upstream environments, alluvial fan flooding takes two mixed-fluvial forms of flooding. Firstly as mud flows and secondly in the form of sediment mixed mode structures such as debris flows. The severity of these forms was demonstrated in Vargas, Venezuela. In December 1999, heavy rain storms triggered alluvial fan flooding that caused the death of approximately 30,000 people and over USD1.8B in damages (Wieczorek *et al.* 2001)

Flood modelling has contributed to predicting and assessing risks and vulnerability (Hunter, N. M. *et al.* 2007). However, accurate assessments have to consider the process mechanisms that distinguish one event from another within the environment of study. In addition, the type of flooding must be taken into consideration. The viscosity and composition of debris and mud flows are much different than regular flooding. In determining flooding hazards Bello et al. (2003) indicated that mud flows can occur within a 5-50 year return, however larger 100 year return event usually have too much water compared with the available sediment material to sustain long duration mud flows. The unpredictability of composition, viscosity, erosion and sedimentation leads to the general problem of unpredictable flow paths when modelling. Although there are flood modelling and mud flow modelling software, both behave differently within separate boundary conditions. The US National Research Council (NRC 1996) approaches flooding as a process that can include the debris and mud flow, rather than making a clear distinction between both. This simplified approach is preferred from a planning, hazard and risk assessment because of the spatial and temporal uncertainty of the occurrence of precursor events such as landslides that produce the materials for debris and mud flow.

For the purpose of this study, the Faucon watershed and alluvial fan within the Barcelonnette Basin and located in the Southern French Alps is investigated. The site has experienced two major debris flows since the mid-90s, and is of particular interest to researchers.

1.2. Research Problem

Alluvial fan flooding is multi-hazard in nature. Although it is caused by precipitation, as with other forms of flooding, alluvial fan flooding are usually rapid flows and can include debris and mud flows. The occurrences of debris and mudflows during flooding are caused by the transport of dislodged sediments in the upstream from events such as landslides and earthquakes. If the main channel becomes blocked by such sediment material during one event, a later event increases the risk of channel migration as water would seek a path of least resistance. Deprived of sediments, the water would scour the landform. Such events are natural in the development of alluvial fans but pose a problem for people living on alluvial fans and those entrusted to ensure public health and safety.

Modelling of flooding has substantially improved in recent times, however, flow blockages and terrain inaccuracies may present uncertainties in the models. Alluvial fan flood modelling is considered to be greatly influenced by such uncertainties. These ambiguity in flood models that result from the uncertainties is referred to as "unpredictable flow paths" caused by the terrain features, including the deposition of sediments during an event (NRC 1996; FEMA 2000). This study investigates the influence of terrain model uncertainties on flood concentrated flow paths.

1.3. Research Objectives and Questions

The project seeks to determine the sensitivity of DTM uncertainties to flood hazard model assessments. As flood modelling is dependent on the study environment, it is imperative that triggers, causes and consequences be considered. In order to achieve this, the following sub-objectives and related research questions are investigated:

- To perform rainfall runoff modelling to predict a 100 year hydrograph for the study area
    - What is the influence of infiltration and water storage parameters on the runoff?
    - Does the hydrograph represent typical flood inducing storm events?
- To make flood hazard maps for debris flow channel infilling scenarios
    - Can flooding occur during a 100 year event without blockages or infilling?
    - Which areas on the channel are sensitive to breaching in the event of infilling??
    - Which areas on the alluvial fan are sensitive to flooding?
- To evaluate the sensitivity of flood hazard mapping based on different terrain expressions
    - How sensitive is modelled overland flow to terrain inaccuracies?
    - Where on the alluvial fan is there risk of high impulse?
    - Is there systematic flood patterns resulting from scenarios and uncertainties?

1.4. Research Hypothesis

The following hypothesis in anticipation of the results of the study:

- Uncertainty in rainfall-runoff modelling is predominately affected by uncertainty in soil infiltration.
- The amount of discharge during a 100 year rainfall event is not significant to cause flooding in the absence of blockages.
- Inaccuracies in the DTM can significantly alter the modelled flow paths and areas affected by inundation.
- Overland flow paths and inundation patterns cannot be well represented without considering DTM inaccuracies.

1.5. Thesis Structure

This report consist of eight chapters in addition to the list of references:

Chapter 1 outlines the framework of the thesis, the problem, objective and the structure of the research taken by the author in determining the validity of the hypothesis.

Chapter 2 reviews literature on the various aspects determined relevant to the research.

Chapter 3 introduces the reader to the study area and its suitability in determining the objectives of the study.

Chapter 4 outlines the fieldwork and laboratory methodology, and the subsequent results and analysis of the factors required for the various models.

Chapter 5 answers fundamental questions regarding the watershed hydrology. The chapter will detail the methods used and the results in determining the runoff from the upstream areas in the watershed.

Chapter 6 considers blockages, infill scenarios and their effects on concentrated overland flow paths.

Chapter 7 discusses the validity of the methods, results, limitations and deductions drawn.

Finally chapter 8 concludes the research by answering the research questions and overviews the scopes for further studies.

2. Literature Review

2.1. Processes in the Genesis of an Alluvial Fan

The genesis of an alluvial fan is based on three conditions (Blair and McPherson 2009): firstly, a topographic environment in which the upland catchment drains into a valley; secondly, sufficient sediment material to create the fan; and finally a triggering mechanism to dislodge the catchment sediments. Once dislodged, usually by landslides or earthquakes, sedimentary material can be deposited onto the fan by three mechanisms (Blair and McPherson 2009): water as the transport agent in a fluid-gravity process; gravitational forces acting on the sediments, referred to as a sediment-gravity process; and finally, the forces of gravity acting directing on disintegrated bedrock, rock-gravity process. The reader will appreciate that alluvial fans are multi-hazard environments that include: erosion and landslides in upstream; and sediment-laden flooding in the downstream.

Over time the fan will undergo a series of sheet flows and channelled water flows until a structured incised channel is formed as illustrated in figure 1. The incised channel would at times of heavy discharge fail to confine fluvial transport, reverting to sheet flow. During sheet flows, a new channel may be incised as the water channel flow path changes. The fluctuation in the sediment regime over time changes the distribution of materials across the alluvial fan, until the fan reaches a maximum limiting size or the discharge level significantly reduces. Thereafter, channel migration is usually the predominant activity, until the deprived high velocity water scour the underlying sediments to create a more permanent incised channel, at times creating terraces of different deposit compositions (Blair and McPherson 2009; Clarke, L. *et al.* 2009).

Sheet flow occurs at times of heavy precipitation, and is considered to be the inability of the channel to confine the volume of discharge. This form of flooding is a flash flood event, that develops the alluvial fan (Blair and McPherson 2009). However, because of its hydrological characteristics in the transportation of water and sediments it is considered as a special type of flooding. The US National Flood Insurance Program (NFIP) regulations define alluvial fan flooding as: “flooding occurring on the surface of an alluvial fan or similar landform which originates at the apex and is characterized by high-velocity flows: active processes of erosion, sediment transport and deposition; and unpredictable flow paths.” (NRC 1996). As such, three criteria are used to determine alluvial fan flooding hazard (NRC 1996); an unconfined and unpredictable flow path occurring below the apex of a fan; sediment scouring and abrupt depositing from water or debris flow as transportation capacity decreases; and an environment whose geomorphology cannot be altered to mitigate the hazards.

In Faucon, the surrounding badlands, still contribute sediment and the channel still undergoes backfilling. However, mitigation measures including check dams, dikes, channel widening and post debris flow response has controlled severe alluvial fan flooding and hence potential growth of the alluvial fan.

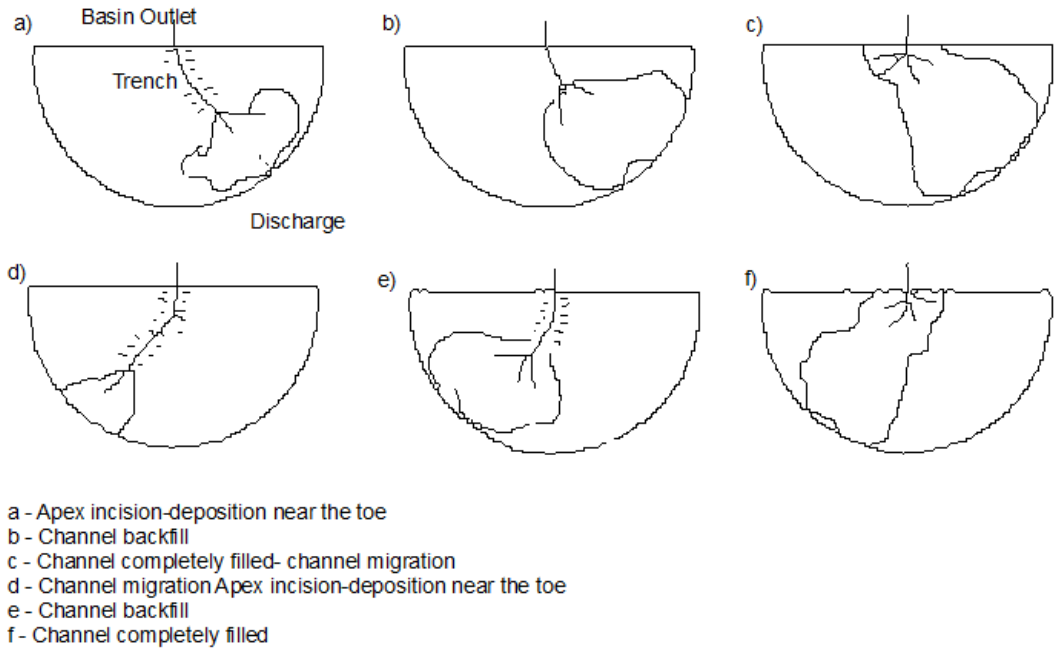

Figure 1 Processes on the Alluvial Fan [adapted from (Schumm *et al.* 1987)]

2.2. Modelling rainfall-runoff

The role of hydrology in the evolution of alluvial fan is wide-ranging. In the previous section hydrology as the fluvial transport agent was mentioned, however it can also be considered as the triggering mechanism for landslides. As mentioned earlier, landslides is one of the main upstream processes that lead to debris flow. The relationship between rainfall, groundwater and slope instability are key factors that are still part of all research into understanding triggers, mechanisms and consequences. However, for the context of this research, only the rainfall runoff relationship shall be investigated.

Hydrologists have developed their understanding of the hydrologic cycle into models. These are based on the observer perceptions of the overall water balance in reference to the scale of observation (Beven 2001). Conceptualization of models can be taken from a very broad, holistic system to a more detailed scale as shown in figure 2. Categorically, these models can be in the context of, stochastic or deterministic, physical or empirical, lumped or distributed, or combinations based on mathematics, input parameters and spatial variability (Moradkhani and Sorooshian 2008). Within each category, modellers make assumptions of parameters (variables) and their inter-dependence, thereby simplifying the reality and the modelling data needed (Moradkhani and Sorooshian 2008). There is no standard regarding the choice of models, parameterization and error estimation (Clarke, R. T. 2008). As such, it is not possible to ascertain the choice of one model over another based on accuracy. Eisenbies *et al.* (2007) remarked that the choice is often driven by preference, politics, familiarity, consistency and availability.

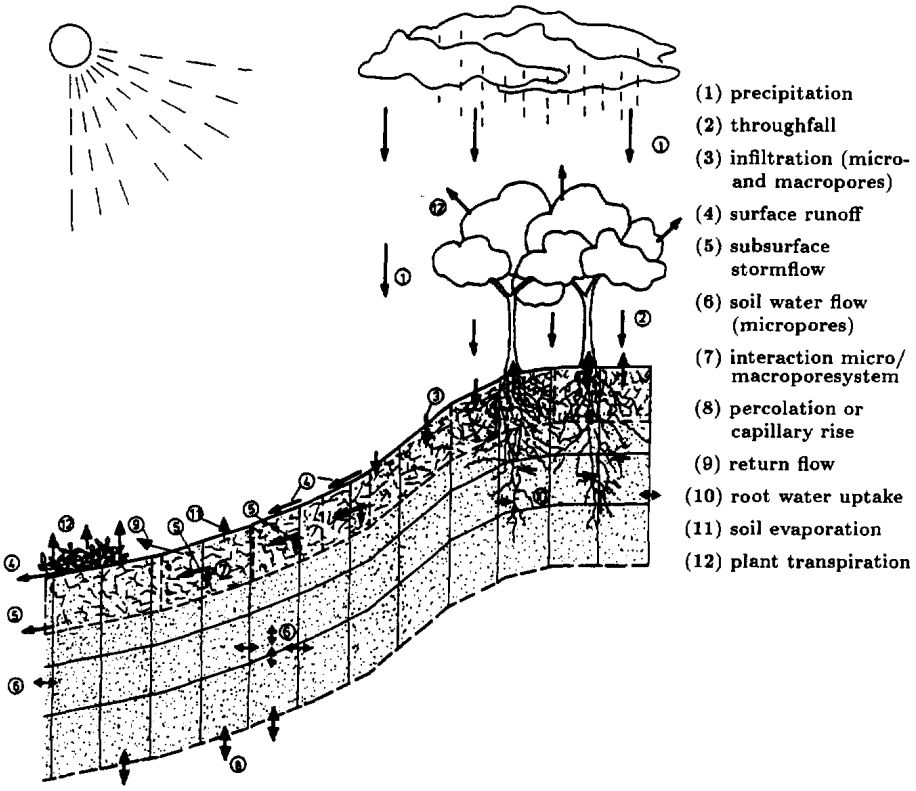

Figure 2 Hill slope and micro-catchment hydrology model (Bronstert and Plate 1997)

In complex environments, the nature of parameterization and data needed, often cannot be represented with a detailed physical model as shown in figure 2 (Bronstert *et al.* 1998). In such circumstances, empirical and statistical methods have been successfully used. The Soil Conservation Service Curve Number (SCS-CN) is one methodology that has been favourably used for discharge modelling in erosion models (Arhonditsis *et al.* 2002; Mishra, K. S. and Singh 2004; Tyagi *et al.* 2008). While its parameterization is few and simplified, it can be adapted to assess catchment runoff (Mishra, S. K. *et al.* 2005). Among statistical methods, the non-linear artificial neural network is an interesting method based on relating rainfall to runoff, without considering parameterization. However, such models exhibit extrapolation problems and thus require vast data input (Lin and Chen 2004; Lin and Wang 2007).

While various mathematical models have been successful, Sivakumar (2008) advocated for the use of simplified models that are specific to the context and location of use, focusing on dominant processes affecting the study. The concept of modelling a wide range of parameters is considered to be susceptible to over-parameterization because non-important parameters remain part of the model, thereby may degrade the quality of results. However, in complex environments, the physical processes may not be truly understood, and poorly relating perceived dominant processes can greatly influence the results and skew the understanding. Parlange and Sander (1985) evaluated one such model and found the results did not reflect the modellers findings. They further concluded that reliance on specific site mathematical models that reflect the specific processes has the risk of incorporating uncertainty through its mathematical modelling, and rather any errors should come from physical model.

It can be argued that one dimensional (1D) physically based models are generally not simple representations of reality. These models can also be considered as susceptible to over parameterization and mathematical uncertainty. However, such models have had favourable outcomes in developing discharge hydrographs for flood modelling. Kuchment (1997) used such models to determine combinations of hydrodynamic factors that can lead to extreme runoff events that cannot be foreseen from historical statistics of rainfall and runoff. In assessing alluvial fan flooding assessment designs, Hamilton *et al.* (1988) recommended the use of 1D models to estimate the discharge of the upper watershed of alluvial fans, for design storm events. Hamilton considered this as a feasible option when working in arid regions and data-lacking environments.

The term 1D refers to the method, and relevant equations used to rout water in the model. For example, the Limburg Soil Erosion Model (LISEM) uses the kinematic wave to concept to model distributed overland and channel flow routing (Jetten 2002). The kinematic wave concept is based on the law of conservations and a flux-concentration relation (Singh 2002). Singh continued to explain that coupling of these two equations implies that the flow of water is in the downstream direction and cannot model backwater flow. The typical flow directions in 1D modelling is shown in figure 3.

For alluvial fan flooding, the recommended data requirements are peak discharge, flow duration and flood volume in the form of hydrographs (Hamilton *et al.* 1988). LISEM can derive these factors based on rainfall intensity and four categories of derived factors: DEM derived factors such as slopes; landuse derived factors such as runoff friction (manning's n); soil type derived factors such as infiltration capacity; and impermeable areas such as roads (Smith and Ward 1998; Jetten 2002). In this study, LISEM is used to combine DEM factors with physical variable factors, such as infiltration, to determine the discharge related information from the upper catchment.

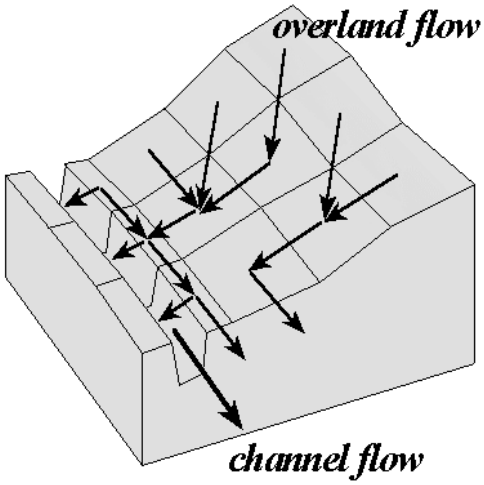

Figure 3 1D Overland flow and Channel Flow
(Jetten 2002)

LISEM is a physically based hydrological and soil erosion model integrated into a Geographic Information System (GIS) (De Roo *et al.* 1994). LISEM uses PcRaster as its GIS platform. PcRaters is a numerical spatio-temporal GIS that allows controlled hydrologic process modelling (Svetlitchnyi *et al.* 2003; Schmitz *et al.* 2009). LISEM is designed to be flexible with the data requirements that can be generated from general base maps. Both LISEM and PcRater are freely available to the public.

2.3. 1D, 2D Surface runoff modelling

Unlike 1D runoff modelling, 2D models can provide a more accurate assessment of spatial and temporal routing of overland flow. Both 1D and 2D models are based on kinematic wave approximations to the Saint Venant equation, however the former is a first order differential solution (Singh 2002; Howes *et al.* 2006). In Digital Elevation Models (DEM) 1D models are solved by the analysis of each cell to determine the flow vectors to one of the eight adjacent cells, and assigning the vectors to a local drainage direction (ldd) file. 2D model designs differ from this concept by firstly using a second order approximation of the Saint Venent equation and secondly by computing the vectors at each time step rather than the use of an ldd file (Howes *et al.* 2006). However, the time step methodology requires much more computational power and takes longer to solve than the 1D model.

Some software use a coupled 1D2D systems to incorporate both functions. Sobek is an example of a 1D2D system. It uses a staggered grid calculation methodology. Flow is first computed at grid nodes using the 1D model, thereafter the momentum equation is used to calculate flow between connecting points (Laguzzi *et al.* 2001). Within this system, each grid cell is replaced by a node representing the flow depth having four pseudo branches as shown in figure 4. As seen, dX represents the grid size, h_1 and h_2 are water depths at the respective grid, u and v represents flow velocities in the x and y directions, and Q represents the resulting discharge flow in the 1D branch.

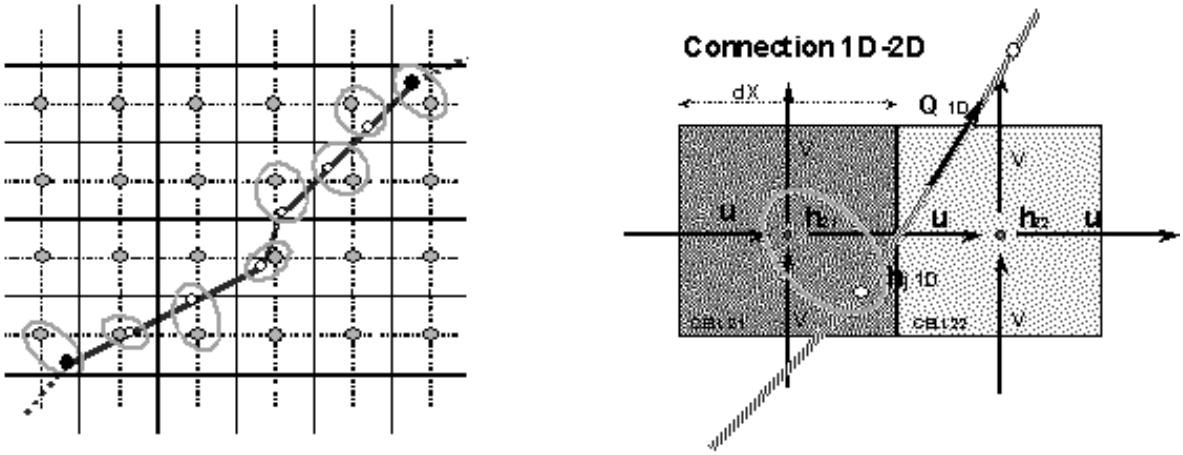

Figure 4 Sobek Overland and Flow Model (Laguzzi et al. 2001)

2.4. Flood Modelling

In the assessment of flood hazard, six characteristic maps based on the water height and velocity are considered important (Alkema 2003): maximum depth, maximum velocity, maximum impulse, maximum speed of rising; duration and arrival time of the flood waters. However, on the alluvial fan the depth, velocity, impulse and blockages are considered specifically important (Hamilton *et al.* 1988). Impulse is a derivative of the water depth and flow velocity given by the product of both (Alkema 2003). These characteristic maps are obtained through hydrodynamic flood modelling. Under overland flow and back flow conditions, a 2D model is required.

In alluvial fan flooding circumstances, the channel is breached and the flow paths are considered unpredictable. Under this condition, 1D models are insufficient, and 2D modelling is required to model such high dynamic flow processes (Hamilton *et al.* 1988). Processes characterized by varying initiation points, unconfined sheet flow, multidirectional flow, hydraulic jump and inundations of multiple channels are synonymous with alluvial fan flooding. Carrivick (2006) showed the suitability of 2D models by using Sobek to reconstruct a high magnitude outburst flood event characterized by the previously mentioned processes.

While 2D models can suitably model flood events, its ability to truly capture alluvial fan flooding is questionable because of the changing terrain surface that occurs as debris is deposited during the process. In experimental models, trench locations during migration events show the uncertainty that mud and debris deposits can have on the flow paths as shown in figure 5. Not only does the flow paths change, but also exhibit deviations from an expected down slope direction. Schumm *et al.* (1987) explained this is due a reduced flow momentum as the water acts against gravity.

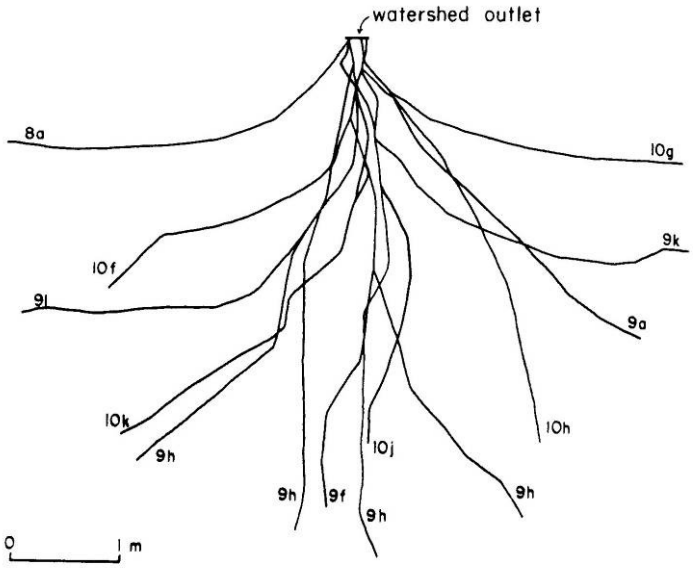

Figure 5 Results of experimental alluvial fan trench paths (Weaver 1986; Schumm *et al.* 1987)

Similar unsystematic flow paths structures have been found by authors who tested flow paths changes in relation to DEM sensitivity in terms of resolution and noise. Horritt and Bates (2001) found that higher resolutions were not always better, with both showing similarities. Wu et al. (2008) found that there was no systematic flow paths defined with changing DEM resolutions. Wise (2007) found that runoff patterns significantly varied with DEM sensitivity, by adding noise (artefacts) to the terrain. As such, the rational for adding noise can be summarised as follows:

- The DEM/DSM has inherent systematic and random errors such as slope position (projected horizontal and vertical), georeferencing and footprint (source dependent) (Hodgson et al. 2003);
- The choice of Digital Terrain Analysis (DTA) algorithm to rasterize the vector elevation data created artefacts in the DEM (Zhou and Liu 2004), however the choice of interpolation techniques is not considered significant (Heritage *et al.* 2009);
- The orientation of the Grid causes directional biases on the slope and aspect (Zhou and Liu 2004);
- Fine errors (noise) cause differences in the surface derivatives, the significance of their errors are application dependent (Oksanen and Sarjakoski 2005);
- DEM accuracy is strongly dependent on the accuracy of the vector data (Heritage *et al.* 2009);
- DEM accuracy is not uniform and is a function of local form roughness including vegetation and landcover (Hodgson *et al.* 2003; Heritage *et al.* 2009);
- The DEM/DSM will have variations due to deposition of sediments, that is part of the reasoning for "unpredictable flow paths";
- Finally, the variation of the DEM/DSM can be used as a sensitivity analysis for validating the model, especially in scenarios that may lacks physical evidence to calibrate or validate the model (Rykiel Jr 1996).

In this study, blockage is considered in two aspects; firstly as debris flow blockage of the main river channel and secondly as man-made expressions on the alluvial fan that may change the flow of water. Channel blockage can be considered in the context of a complete blockage or partial in the form of sediment deposits. The spatial location of simulating a blockage can be evaluated by two conditions: Firstly where the channel slope is within 2-5^{o} (Blair and McPherson 2009); or secondly based on past indicators (events) (NRC 1996). Notable overland blockages include housing developments, levees and general development expression such as drainage, roads, and walls (Hamilton *et al.* 1988)

3. Study Area

3.1. Introduction

This research is based in the Faucon watershed and alluvial fan. Faucon is one of many watersheds, currently investigated in the Mountain Risk Alp Research. The area has been meticulously studied since the 90's and is still studied for its landslides and debris flows hazards. This chapter introduces the reader to the different geographic, social, environmental aspects of Faucon, the data available and the fieldwork done in September/October 2009.

3.2. Geographic Context

Faucon is a small village located within the Haute-de-Alps province in the in the Southern Alps of France, as shown in figure 6. The village is located on an alluvial fan whose upstream watershed is part of the Barcelonnette Basin of the Ubaye Valley.

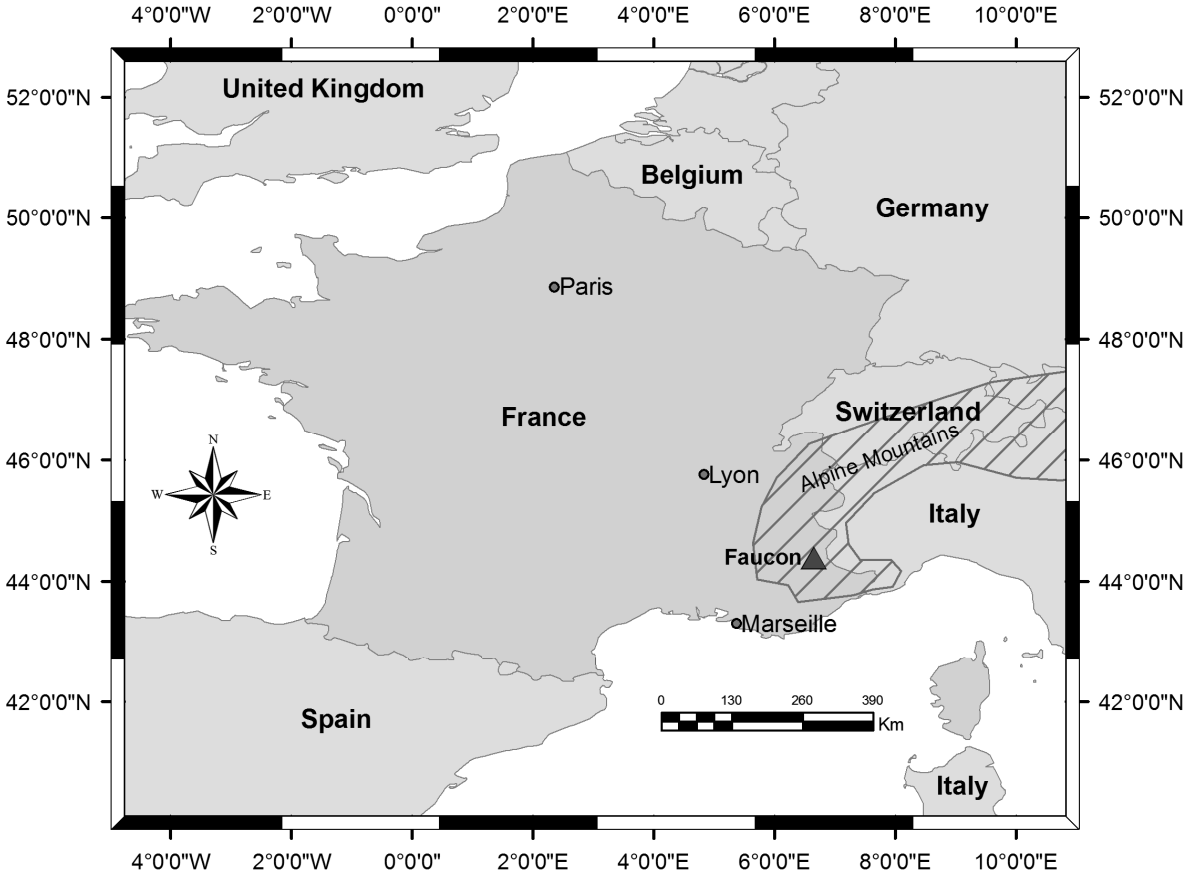

Figure 6 Location of Faucon within France

3.3. Environment

The study area consists of a 9.8km^2 watershed, 5.5 km torrent and a 2km^2 alluvial fan. Elevation vary from 1150m to 2984m with local slopes ranging from 25^o to 80^o at the head of the watershed. The torrent has an average slope of 20^o, ranging from 35^o to 4^o. The slope of the alluvial fan ranges between 4^o to 9^o (Remaitre *et al.* 2005).

The head of the watershed consists of faulted and calcareous sandstones. The central portion is mainly moraine deposits while the lower portion consists of black marl and various quaternary deposits as shown in figure 7. On the alluvial fan, deposits are mainly from debris flow strata (Remaitre *et al.* 2005; 2008).

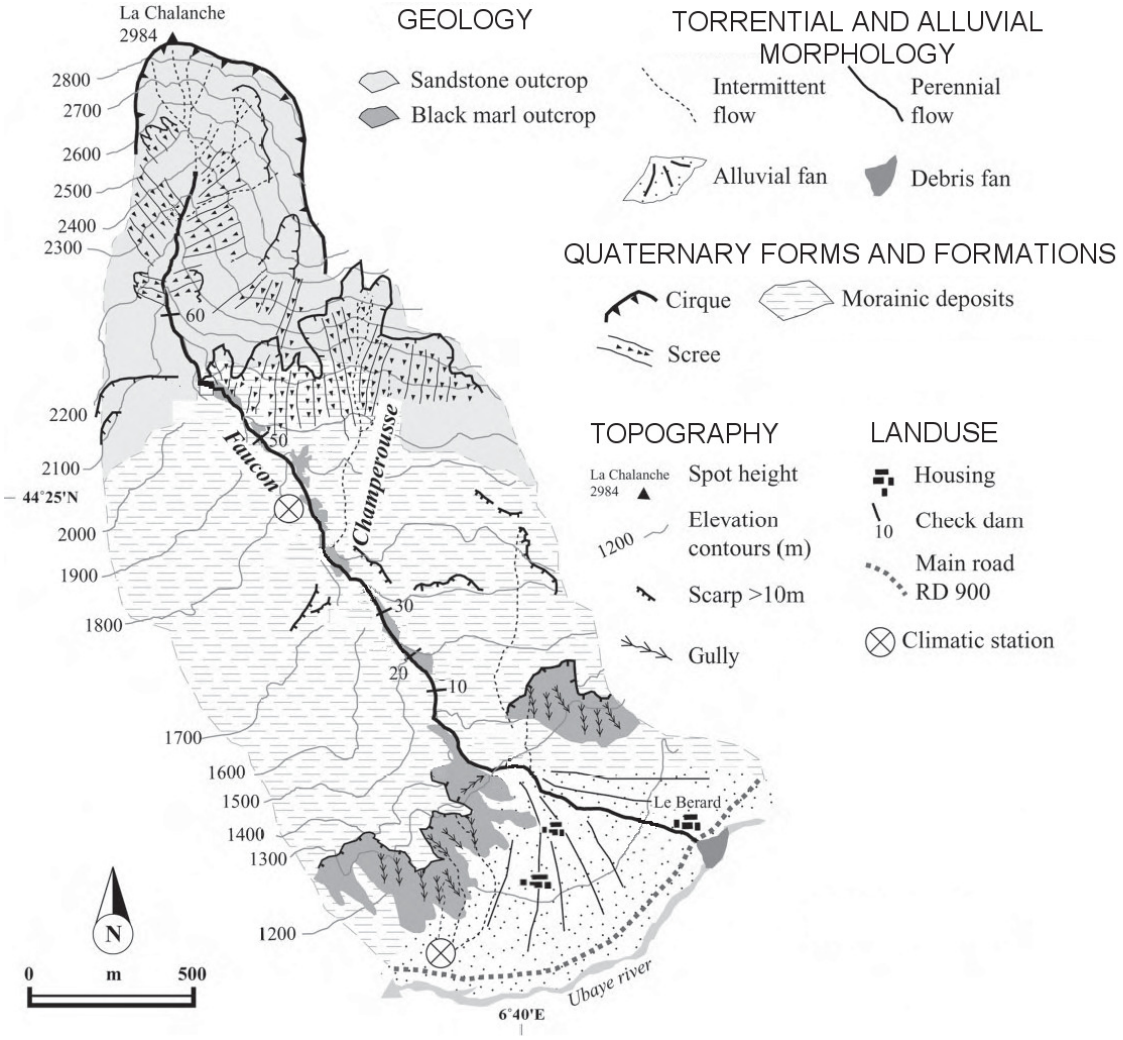

Figure 7 Morphology of Faucon - sensu Remaitre et al. (2005)

The general climate has features of Southern France's Mediterranean regimes on the low elevations but it is attenuated by the mountainous environment. Summers are typically dry with the exception of brief intense storm events; winters are associated with little precipitation in the form of snow, but can have 6 times more snow fall at the higher peaks; spring and autumn are the wettest seasons. Remaitre et al.

(2005) identified that the Faucon discharge from rainfall and snowmelt is typical of the general behaviour of the basin, with rainfall intensities reaching 50 $mmhr^{-1}$. Rainfall variability is influenced by slope and elevation (Weber 1994). The Barcelonnette Basin is said to have approximately 130 freezing days in the year with peak discharge typically occurs during the spring when snowmelt occurs and with high precipitation during the autumn seasons (Remaitre *et al.* 2005).

Landuse of the watershed has been reshaped by mitigation measures following 17^{th} – 19^{th} century human land degradation activity. Housing activity in the catchment is now strongly regulated. Flatter and low gradient terraces in the watershed are used as grazing fields. With the exception of very steep grades, trees have been planted on most slopes. Housing on the alluvial fan consists of a mixed agricultural based village in the centre of the fan and a small non-agricultural community on the east side of the torrent. Agriculture is the predominant landuse on the alluvial fan.

3.4. Events and Mitigation Strategies

Debris flow and flooding have traditionally been problematic in the Alps. Descriptions of torrential floods in Europe, including the Alps, can be found in early literature such as Lhudy (1708). Such accounts describe the wariness of rain by local residents, including precursor observations of their surroundings. Such precursors include colour of clouds, the location of clouds on certain hills, the directional entry of clouds into valleys, and "noise and murmuring of torrents".

The Barcelonnette Basin has experienced at least 561 torrential related events between the periods 1850 to 2005. Of these events, Faucon was affected by 18 debris flow and 41 torrential flood events (Remaitre and Malet 2009). During the last two decades, two debris flows in 1996 and 2003, and one torrential flood in 2002 occurred (Remaitre *et al.* 2005; Remaitre *et al.* 2008). The type of debris flows in Faucon are said to be triggered by two mechanisms, either from liquefaction of landslide debris or with the failure of coarse debris material at higher altitudes or gully bed (Remaitre and Malet 2009).

Since the late 19 century mitigation projects have tried to prevent or reduced hazards in the French Alps. The demand for timber during the 17^{th} century led to deforestation and subsequent expansion of arable lands. The effects of which led to lands degradation thus exacerbating torrential related disasters. Following a major hydrologic event in 1856, the French Government enacted a bill for promoting projects in sediment control and related disaster mitigation. The project, known as the *restauration des terrains en montagne* (RTM), oversaw reforestation efforts, flood hazard, debris flow and landslide mitigation works as shown in figure 8 (Yamakoshi 2004; Remaitre and Malet 2009). It is through the RTM that much of Faucon's watershed slopes has been reforested and over 100 check dams built to control debris flow, landslides and flooding.

Figure 8 Check dam in the Faucon torrent amidst degraded landscape, pictured from 1901(OMIV-EOST 2009)

3.5. Data Available

The data available from the Mountain Risk Project includes much of the Barcelonnette basin, and over 10 years of research data. Table 1 shows the data used in this project. The data includes daily information precipitation data from the Barcelonnette climate station during the period 1928 to 2004, and hourly precipitation for the Faucon rainfall station from October 2001 to September 2003. Most of the data lacked metadata, and when available was in French. However, the data within the project are continuously updated. Base maps have been included in appendix I.

Table 1 Data Available from the Mountain Risk Project

Data	Data Type	Remarks
Climate	Time series	In French
Hydrologic Report	Document	In French
Torrent	Shapefile - vector	
Roads	Shapefile - vector	Including but not distinguishing tracts
Soil depth	Shapefile - polygon	
Soil Map (morphology)	Shapefile - polygon	
Landuse	Shapefile - polygon	11 classes based on 2004 imagery
Boundary	Shapefile - polygon	
Buildings Footprint	Shapefile - polygon	
2003 Debris Flow	Shapefile - polygon	With deposit depths
DEM – 10m res.	Raster	

3.6. Data Collected During FieldWork

Data acquisition was conducted from September to October of 2009. The data acquired included fieldwork and secondary source information. Table 2 shows the type of data collected, its source, and its intended purpose.

Table 2 Data and Information Acquired during Fieldwork

Data/information Type	Source	Purpose collected
Hydraulic Conductivity	Field/Lab Observation	Use in the runoff modelling
Porosity	Lab Observation based on soil samples	Use in the runoff modelling
Initial Soil Moisture	Lab Observation based on soil samples	Use in the runoff modelling
Soil Depth	Field Observation	Use in the runoff modelling
Soil Texture	Field Observation	Reference in runoff modelling
River Cross Sections	Field Observation	runoff modelling
Alluvial Fan Blockages	Field Observation	runoff modelling
Misc.: Surface and soil characteristics	Field Observation	Reference
Misc.: hydrologic	Remaitre (2009)	Reference
River Survey	Municipality	Reference

4. Fieldwork and Laboratory Analysis and Results

4.1. Introduction

As stated previously, fieldwork was conducted during September/October 2009. Subsequent lab-work and analysis of data required for the modelling was done in October/November. This section outlines the fieldwork, lab-work and the results of the main factors used in the runoff modelling.

4.2. Watershed Measurments and Observations

4.2.1. Sampling and Saturated Hydraulic Conductivity

Saturated hydraulic conductivity (Ksat) was measured using three techniques. This consisted of the use of standard pF rings (Ø53x50mm), single ring infiltrometer method using the falling head principle with a Ø12cm ring and the constant head principle with a Ø53mm ring.

Based on landcover patterns, 44 observations were acquired from 27 locations as shown in figure 9. These included 24 pF samples, and 20 (8,12) single ring infiltrometer readings. Sampling was not done on steep slopes including the bare rock area on upper part of the watershed and the black marls. Steep slopes also limited the sampling position within the forested areas. Accessibility to private property also limited the sample locations.

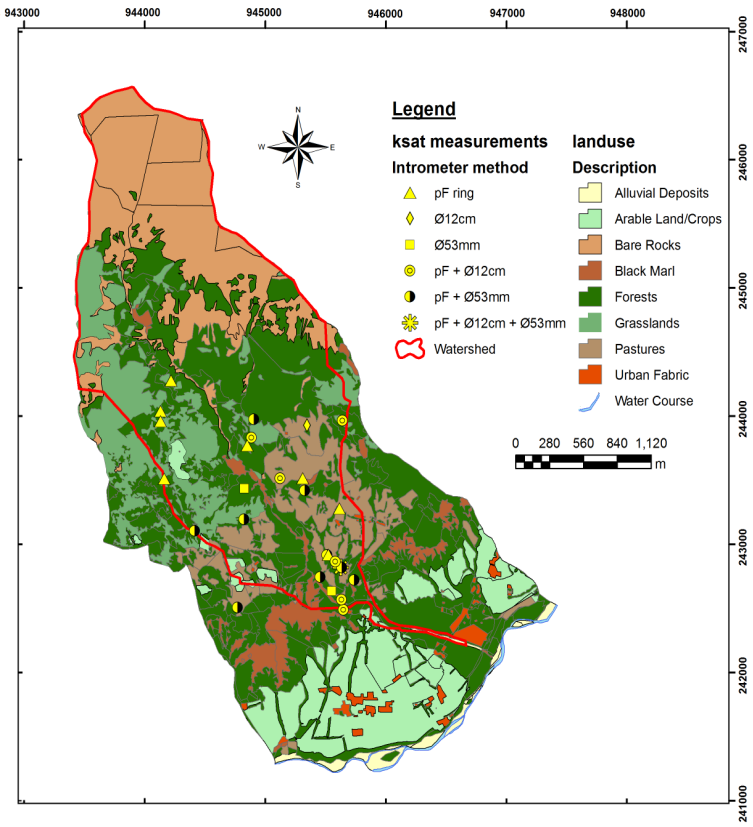

Figure 9 Sampling locations in reference to landcover

Standard practice was applied in the extraction of field samples. Sampling was done only on the top soil layer using standard pF equipment, following the procedure outlined by Eijkelkamp (2009b). However, because of high gravel contents and dry soil conditions, sample locations were moistened before extraction. This was done for two reasons: to reduce the force required driving the sample, thus limiting ring damage; and to increase the soil cohesion which otherwise crumbled during extraction.

Single ring infiltrometer was a field decision following failed double ring infiltrometer testing. The double ring infiltrometer was found to be impractical for two reasons; firstly, driving the cylinder to the required depth of 5cm (Eijkelkamp 2009a) was not possible because of technical and field conditions; and secondly, the water required to fill both cylinder was not practical. Alternatively, the inner ring was used in isolation; however, the water problem still demanded another alternative sought in the use of a smaller ring requiring less water.

The inner ring was measured using a falling head methodology. The ring was placed approximately 2cm into the ground (depth of insertion recorded). A measuring rule was placed in the cylinder. Water was slowly poured into the ring until a slow infiltration was attained. A starting reading level on the rule was determined, and the water in the cylinder was topped up to the chosen mark. From this mark, the rate at which the head decreased along the measuring rule was recorded, as shown in figure 10.

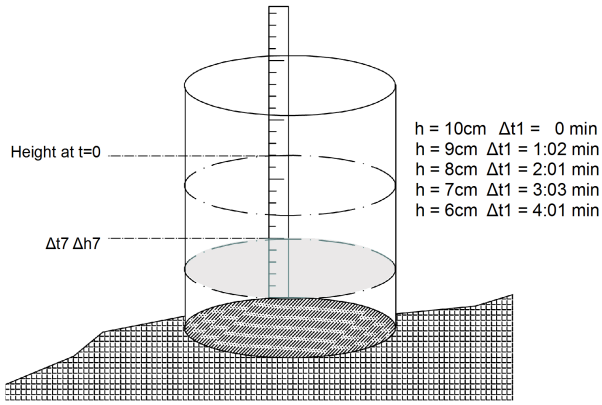

Figure 10 Falling head single ring infiltrometer method

Unlike the measuring falling head method used for the larger ring, the constant head methodology was used for the smaller ring, as depicted in figure 11. This was done by carefully driving the pF ring into the ground with the hammer and driver. The depth of insertion was recorded. The ring was filled with water and a ponded head was maintained using the measuring cylinder. The time between consecutive emptying of the measuring cylinder was recorded using a stop watch. The readings were then converted to simulate the falling head method by equating the volume added to decreases in height. For a 10cc reading at Δt1, the virtual height (*dh*) will be given by:

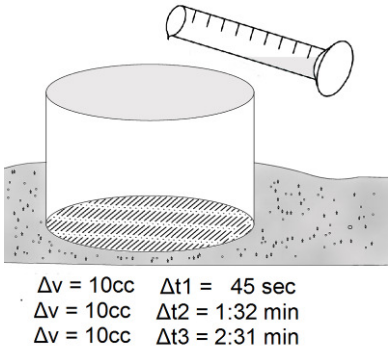

Figure 11 Constant head single ring infiltrometer method

$$dh = \frac{\Delta v}{\pi r^2} \qquad (4.1)$$

Where Δv is the volume at Δt1, Δv = 10cc, r is the radius of the ring (2.5cm), which gives dh = 0.5 cm. The rate of water flux can be calculated from the average of $dh/\Delta t$, or plotting the cumulative dh against cumulative time and defining the water flux as the slope.

To reduce the measurements of the single ring infiltrometer, the calculation outlined in Wu *et al.* (1999) was used as given by:

$$K_s = A/(af) \qquad (4.2)$$

Where A is the slope corresponding to the rate of water flux in cm/min, a is a dimensionless constant (a = 0.9084), and f is also dimensionless and given by:

$$f = \frac{H + \frac{1}{\alpha}}{G^*} + 1 \qquad (4.3)$$

Where H is the ponded depth in the ring in cm, α is a coefficient of the soil texture ($\alpha = 0.04$ cm^{-1} for clays), and G^* is a function of the radius of the ring (r) in cm, and depth of insertion (d) also in cm, given by:

$$G^* = d + r/2 \qquad (4.4)$$

4.2.2. Soil Depth

Field measurement of soil depth was found to be generally impractical due to equipment and field conditions. The Edelman auger was found to be unsuitable for the gravelly/stony environment and the general moraines deposits. Soil depth measurements from road cuts were also not feasible because of the fragility of roads embankments as shown in figure 12. With few exceptions, small pits were dug at the pF sample locations shown in figure 9, to give an understanding of soil stratigraphy as shown in figure 13. More details regarding this information is shown in appendix II.

Figure 12 Typical road cut with loose rocks including boulders

Figure 13 Pit dug for soil depth analysis

4.3. Alluvial Fan Measurments and Observations

4.3.1. Cross Sections

Cross sections were measured for the river channel along the alluvial fan. This was required for the 1D part of the hydrodynamic modelling in Sobek. The cross section were measured by measuring the bed width using a digital measuring tape/or a pocket tape depending distance to be measured. The slope angles, on each bank were measured using a clinometer. Finally, the slope distances, of the banks, were also measured using the digital meter/pocket tape. Off site, the measurements were reduced using trigonometry to calculate grade and width between banks, for use with Sobek. The various measurements are depicted in figure 14.

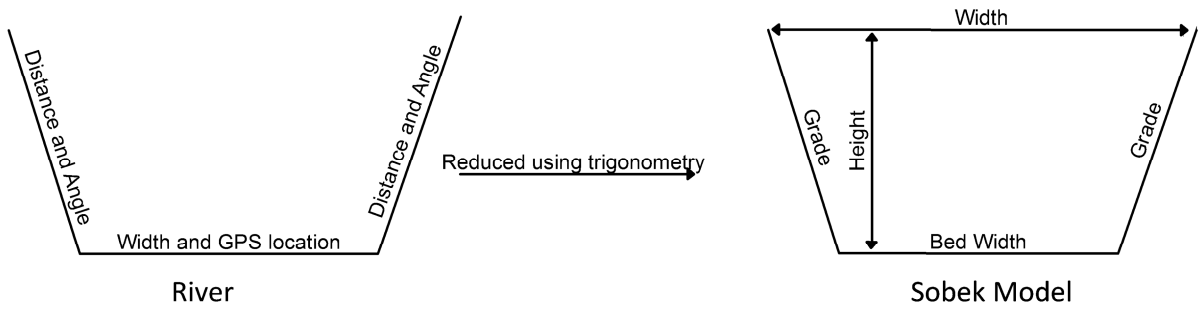

Figure 14 Cross section measurements and post-field reduction

4.3.2. Alluvial Fan Blockage Survey

An observational survey of the features along the alluvial fan that may inhibit or redirect the water was done. Two of the major sources of flow blockage on the fan; the buildings and dikes, were already obtained from secondary sources. The other factors that were considered included roads, walls, terrain. However, this was limited because of the type of survey and equipment required.

4.4. Laboratory Measurements

Ksat, porosity and bulk density were determined from the pF ring samples. Some of the pF samples were processed pseudo-field, to determine the Ksat values. This was done using a simple measuring cylinder, funnel and water bottle to simulate the constant head method condition, as shown in Figure 15. Reduction was done by using Darcy's law as given by equation 4.4. Q is the gradient of the volume (cm^3) measured per unit time (min), A is the cross sectional area (cm^2), L is the depth of soil sample (cm) and dh is the depth of the pounded water (cm). *Ksat* was computed in cm/min but later converted to mm/hr.

$$Ksat = \frac{Q}{A} \times \left(\frac{L}{L + dh} \right) \qquad (4.4)$$

Samples acquired during the last week of field work were processed in the laboratory using a permeameter, following the standard equipment and instructions (Eijkelkamp 2008) . For cross verification, some of the previously measured samples were also re-measured using the permeameter. Both Ksat measurement techniques required the pre-saturation of samples and all results were reduced to mm/hr.

Porosity was obtained from the difference between the dry and saturated weights of soil samples per canister volume. This was done by using the saturated weight (W_{sat}) and the dried weight (W_{dry}), both samples included the weight of the rings in grams and converted to ml. The drying of the sample was done in an oven at 105° for 24 hours. The porosity was computed as a dimensionless percentage using equation 4.5, where V is the volume (ml) of the cylinder.

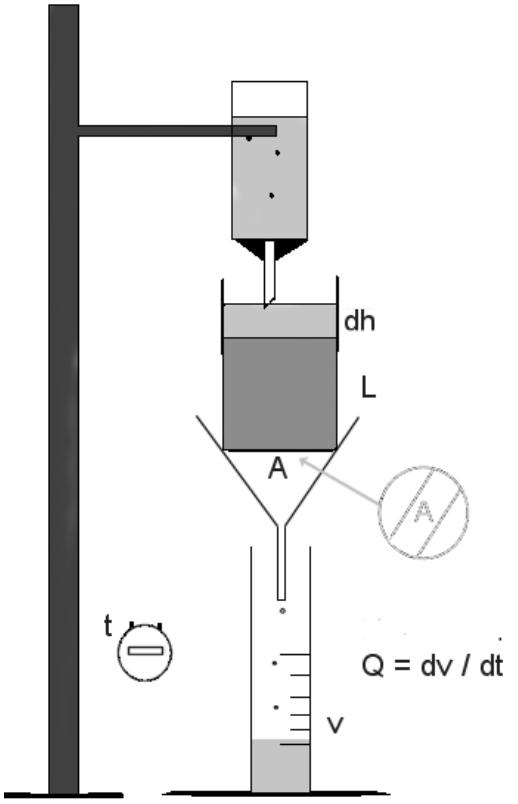

Figure 15 Pseudo Lab Method used for Ksat Measurements (Alkema 2009)

$$P = \frac{W_{sat} - W_{dry}}{V} \times 100 \qquad (4.5)$$

Bulk density was also measured from the dry sample as a percentage of the volume of the pF ring using equation 4.6. However, the dry soil weight W^{*}_{dry} excluded the weight of the pF ring. In this calculation, bulk density was calculated in g/cm3, as units of weight and volume were not converted to ml.

$$B_{\rho} = \frac{W^{*}_{dry}}{V} \qquad (4.6)$$

Soil moisture at sampling was measured as a percentage of the difference between soil weight, before saturation, to the oven dry sample per canister volume as given in equation 4.7, where W_{int} refers to the initial soil sample weight before saturation. All measurements were used in ml, and *Pi* calculated as a dimensionless percentage.

$$P_i\% = \frac{W_{\text{int}} - W_{dry}}{V_{soil}} \times 100 \qquad (4.7)$$

4.5. Results and Analysis

The results presented below are aggregated results. The reader is referred to appendix II for the complete list of results including a location map of sampling locations. Detailed results include Ksat, texture, porosity, bulk density, soil moisture, soil colour, gravel content, soil depths, and general remarks of the pF samples. Results of the cross sections along the torrent and at bridges are presented in chapter 6.

4.5.1. Saturated Hydraulic Conductivity

In total, 43samples of Ksat was observed, however 4 were rejected for having values larger than 1000 mm/hr. The pF values repeated using the permeameter were also rejects since the RMS was found to be more than 2000mm/hr. In most cases the repeated values were less than the pseudo-lab measurements. The aggregated results of the remaining 39 samples are shown in table 3 and figure 16 with reference to different mapping units.

Table 3 Summarized statistics for the Ksat observations

Mapping Unit	Sub-unit	mean (mm/hr)	sd (mm/hr)	median (mm/hr)	n
Land-cover	Forests	252	184	191	19
	Grasslands	150	90	142	8
	Pastures	58	78	37	13
Morphology Units	Flyschs	434	234	525	4
	Moraines	117	118	66	31
	Torrent. Dep.	118	-	188	1
	Weath. Marl	296	78	316	4
Soil Texture	Clay	178	164	175	6
	S. Clay	180	168	133	25
	S. Clay Loam	130	160	47	9

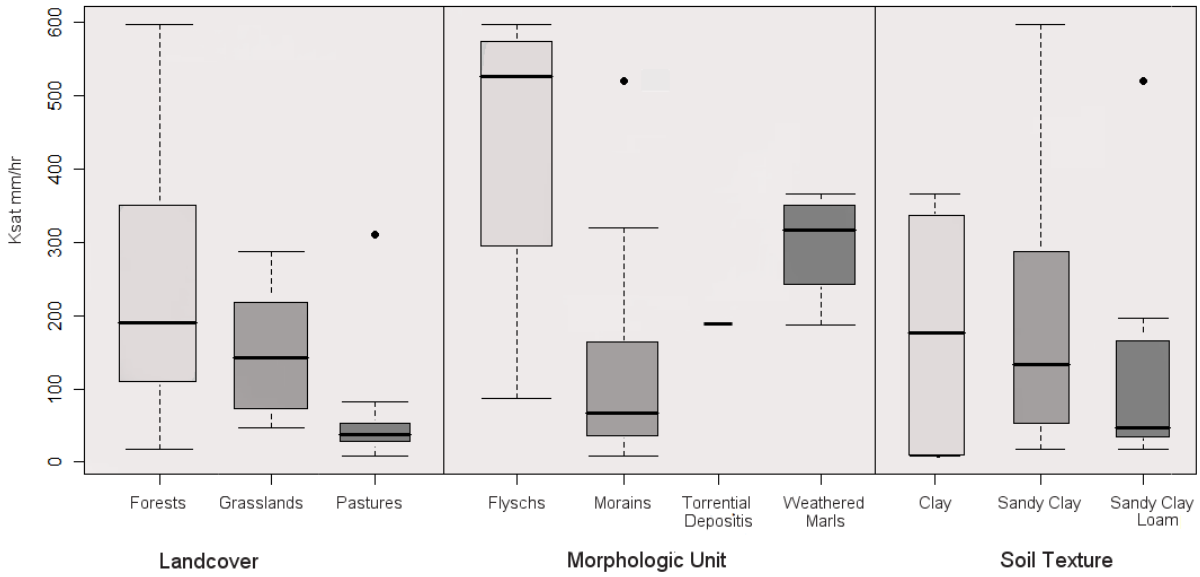

Figure 16 Comparison of Ksat results by mapping units

The Ksat values as shown in table 3 and figure 16 showed a more discerning distribution with the morphology units, although their values are relatively high compared to landcover and soil texture. However, their ranges were similar to a previous study (Remaitre 2006), who used a rain simulator technique to measure the infiltration. Further exploration of the data showed that grouping by landcover and measuring technique, as shown in table 4 and figure 17, revealed contrasting differences between methods.

Table 4 Summary of Ksat results by collection method for landcover sub-units

Method	Sub-units	mean (mm/hr)	sd (mm/hr)	median (mm/hr)	n
Small rings	Forests	60	24	58	4
	Grasslands	73	10	73	2
	Pastures	40	30	36	5
Larger rings	Forests	364	170	331	4
	Grasslands	121	NA	121	1
	Pastures	45	16	37	3
pF lab tests	Forests	296	180	255	10
	Grasslands	186	96	166	5
	Pastures	99	141	39	4

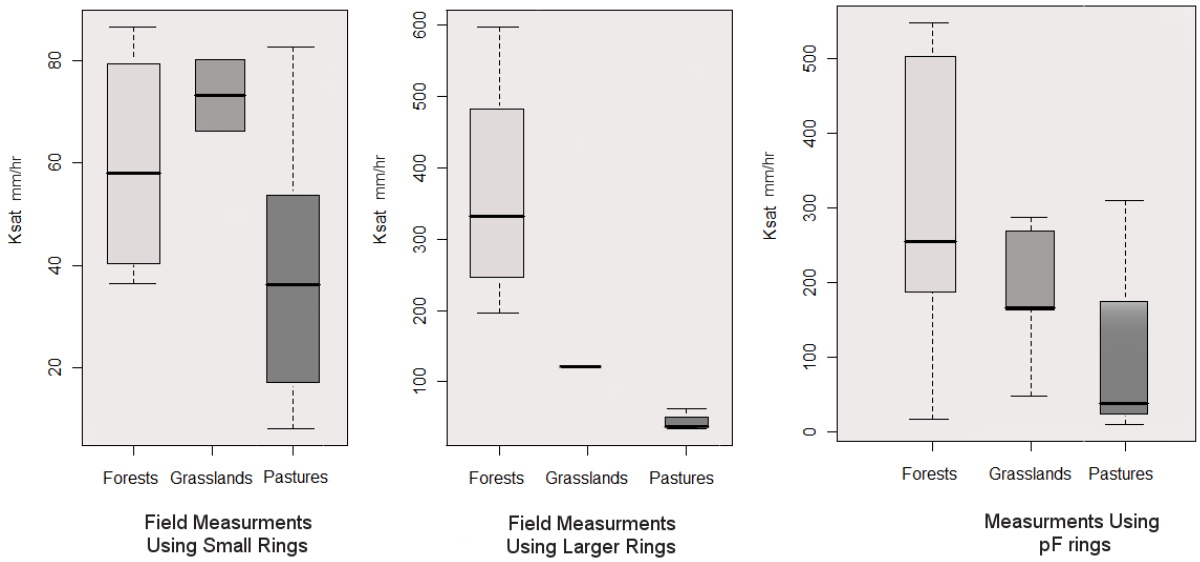

Figure 17 Comparison of different methods for Ksat measurements

4.5.2. Porosity, Bulk Density and Initial Soil Moisture

The results of the porosity and bulk density tests were also grouped by different mapping units as presented in table 5 and depicted in figure 18. Finally, results of the soil moisture content are shown in table 6.

Table 5 Summarized statistics for the porosity and bulk density observations

Mapping Unit	Sub-units	mean (%)	sd (%)	median (%)	n
Landcover	Forests	54	7	52	13
	Grasslands	59	8	62	5
	Pastures	50	7	49	6
Morph. Units	Flyschs	54	8	54	2
	Moraines	54	8	52	19
	Torrent. Dep.	52	-	52	1
	Weath. Marl	56	4	57	2
Soil Texture	Clay	60	1	59	3
	S. Clay	53	8	52	16
	S. Clay Loam	52	8	50	5
		Bulk Density (g/cm^3)			
Soil Texture	Clay	1.79	0.08	1.76	3
	S. Clay	1.68	0.58	1.81	16
	S. Clay Loam	1.71	0.43	1.53	5

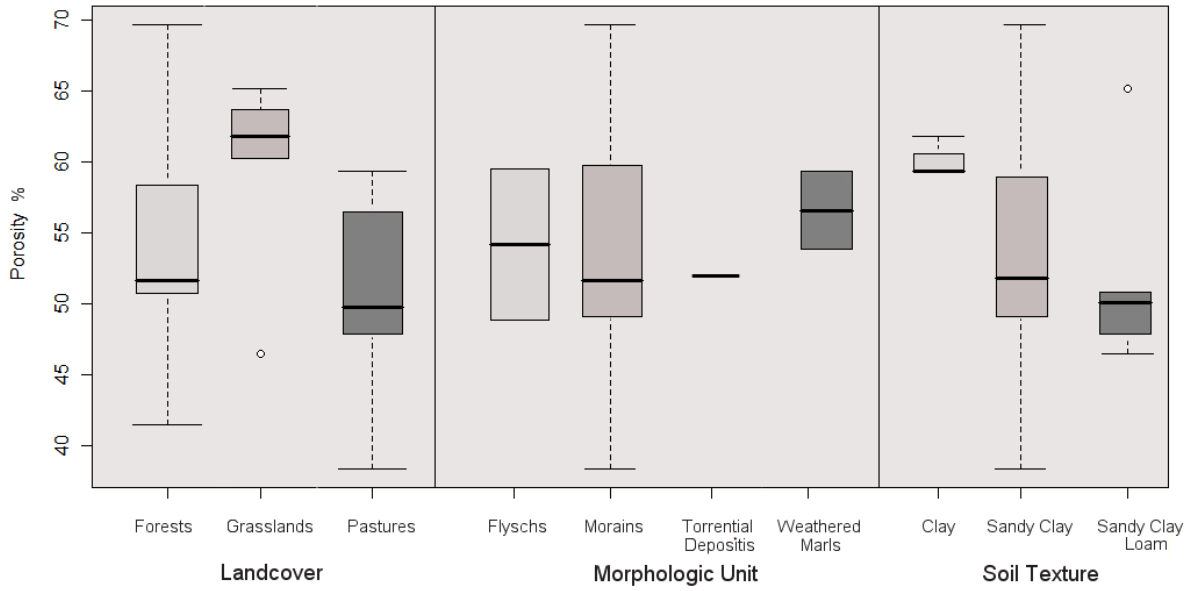

Figure 18 Comparison of porosity by mapping units

Table 6 Initial Soil Moisture Content

Sample #	Initial Soil Moisture %	Soil Texture	Landcover
4	55	Sandy Clay	Forests
1	54	Sandy Clay Loam	Pastures
19	54	Sandy Clay	Grasslands
11	48	Sandy Clay Loam	Pastures
21	48	Sandy Clay	Forests
2	46	Sandy Clay	Grasslands
12	45	Clay	Grasslands
1	40	Sandy Clay Loam	Pastures
13	36	Sandy Clay	Forests
7	31	Clay	Pastures
23	30	Sandy Clay	Pastures
6	28	Sandy Clay	Pastures
15	21	Sandy Clay	Forests
5	17	Clay	Forests
22	16	Sandy Clay	Forests
	1st Quartile = 29	Median = 40	Average = 38

4.5.3. Soil and Surface Characteristics

As mentioned earlier, the determination of soil depths were found to be complicated because of field conditions. However, field observations found that almost all sites have a base of gravel and soil (with some stones). The percentage of stone, gravel and soil varied depending on the morphology, landcover and proximity to the Flysh badlands. In pasture and bare areas, the gravelly surface is exposed with the surface generally showing signs of sealing and moss covering. The subsurface of these classes was also found to have a higher percentage of gravel and stones increasing with depth. In the grassed areas, the layer is covered by shallow soils, having good structure, ranging from 3 cm to 30 cm. Similarly, in forested areas the gravel layer was also covered, but by an organic layer ranging from 1 cm to 10 cm.

The results of the soil depth investigation revealed a pattern of landscape and landuse as depicted in figure 19. A common deep layer of moraine deposits consisting of soil, gravel and stone was found exposed to the surface in bare areas such as pastures. Grasslands were found to have a developed soil structure covering the moraine structure. Located mostly on slopes, forested areas also had the underlying moraine structure, however covered with a humus layer.

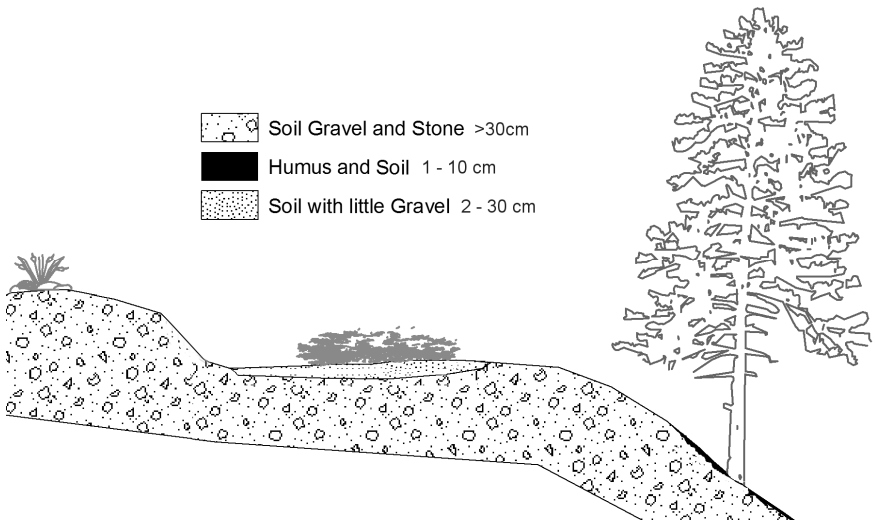

Figure 19 Landscape and Soil depth

4.6. Evaluation of Results

The results showed that the general differences in medians and variations in Ksat can be attributed to equipment, techniques, soil structures, and surface characteristics. The observed Ksat range was considerably lower when using the smaller rings. Such relatively low readings are of the same order as other observations from another watershed within the same Basin by Malet *et al*. (2003). The values obtained by Malet *et al*. were in the range of 10-50.4 mm/hr, using a tension-disk infiltrometer of diameters 250 or 80mm depending on sample location. Van Asch and Buma (1997) also measured low values for Ksat in the order of 6 mm/hr using the inverse borehole method, for yet another watershed in the Barcelonnette Basin.

In contrast to small ranges of Ksat, using the pF and larger single ring, the values obtained were in a similar range to the values obtained by Remaitre (2006). Remaitre studied infiltration in the Faucon watershed at six locations using a rain simulator. The small ring can be considered to lack surface representation as it only samples a small homogenous position. However, the same can be said of the lab measured pF ring samples, which also suppose to be influenced by homogenous conditions. The difference between the field and lab measured Ksat using a small ring and the pF ring, may be because of sealing at the surface. In extracting samples using pF rings, the top layer is removed. The larger ring was a problem to use, lacking proper equipment the soil surface was usually disturbed.

While results were generally different, it is interesting to note that median Ksat results of the pasture landcover were the same for all three methods. It is generally agreed that grazing leads to poor soil structures and reduced infiltration, because of plant reduction and animal trampling (McCalla *et al.* 1984; Bharati *et al.* 2002; Sanjari *et al.* 2006). This poses the possibility that variations in Ksat may also be explained in terms of time lag, regarding landuse changes. Re-growth forests is one transition landuse which showed much different soil structure compared to the natural forests.

In spite of the uncertainties regarding the choice of Ksat values, the decision was taken from a worst case scenario for flooding, to use the lowest infiltration rates, as obtained from the small ring field measurements.

The results of the porosity showed that most of the readings were within the range 48 to 60%. While there were good distinctions between the porosity of soil texture, there were no texture maps. Information based on the works done by Remaitre (2006; 2009) suggests that the soil structure should follow the morphology units as shown in figure 7. However, there is a contrasting difference between porosity plotted by the morphology units and texture. The decision was taken to use the median values associated with the morphology units, since most of the sampling was done on the moraines, and other units are not well represented in the distribution.

It was previously mentioned that pF soil samples were often moisture before extraction. This would have affected the measure of initial soil moisture. As such, the decision was taken to use the lower 1st quartile value of table 6 as an average.

5. Rainfall Runoff Modelling

5.1. Introduction

The objective of this section is to improve on the understanding of the hydrological factors that influence runoff in the Faucon watershed, through physical modelling. As an outcome, a suitable hydrograph is generated for use in the 2D hydrodynamic modelling on the alluvial fan. The models produced here lack validation as two key components have not been obtained: spatially distributed high intensity rainfall data; and discharge data.

5.2. Input Data and Boundary Conditions

The project used various data sources to fulfil the LISEM data requirements. Such data included the field measurements, literature, and estimations from perceptions and observations. Figure 20 shows the base maps used to generate the LISEM maps. Table 7 and table 8 shows the base values used to generate the derivative maps for LISEM, which are considered the base values during the sensitivity analysis. The tables also describe their source values.

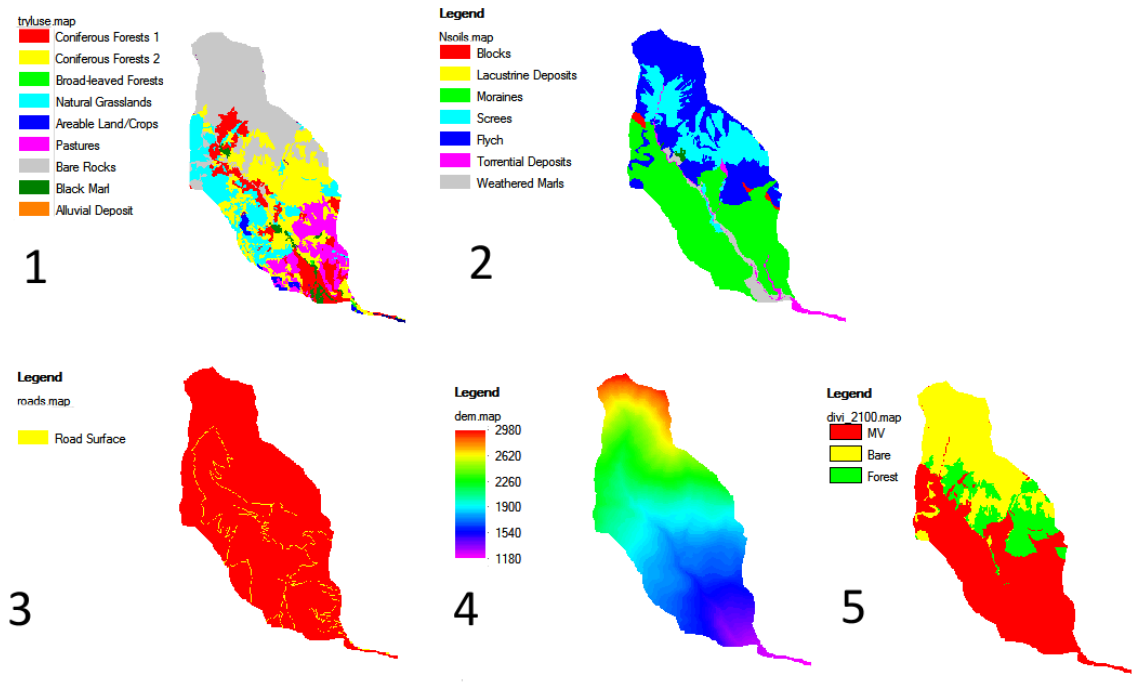

Figure 20 PcRaster Base Maps for use with LISEM: 1 Landcover; 2 Morphology; 3 Road; 4 DEM; 5 Upper forested/non forested maps

Table 7 Values for use with Map 1

Col# 0: ID# Assigned to Landcover Map
Col# 1: Leaf Area Index - calculated from NDVI using Landsat 2004 images using equations by Stensrud (2007); and assigning weighted means to landcover classes
Col# 2: Fraction of Soil Covered by Vegetation - based on field observations
Col# 3: Vegetation Height - based on field observations (m)
Col# 4: Ksat values based on median small ring measurements and literature values (ATF 2010) (mm)
Col#5: Manning's n values based on literature values (Yen and Chow 1984 as reported by Nicklow et al., 2006)
Col#6: Random Roughness based on site observations and Vieux (2006) (mm)
Col#7:Fraction covered with stones - estimated from field observations
Col#8: Fraction covered with crust - estimated from field observations

0	1	2	3	4	5	6	7	8	Landcover Classes	Avg. NDVI
1	2.56	0.1	20	58	0.09	3	0.2	0	Coniferous Forests 1	0.084
2	2.56	0.1	15	58	0.06	3	0.2	0	Coniferous Forests 2	0.106
3	5.1	0.1	20	58	0.09	3	0.2	0	Broad-leaved Forests	0.205
4	0.83	0.75	0.3	73	0.09	3	0.4	0	Natural Grasslands	0.090
5	4	0.75	0.15	36	0.06	3	0.4	0.4	Arable Land/Crops	0.220
6	1	0.5	10	36	0.055	3	0.4	0.4	Pastures	0.080
7	0	0	0	03	0.045	1	0.6	0.4	Bare Rocks	-0.199
8	0	0.1	0	0.1	0.03	3	0.6	0	Black Marl	-0.116
9	0	0	0	40	0.03	3	0.75	0.1	Alluvial Deposits	-0.226

Stensrud (2007) NDVI to LAI:
LAI = 1.5(NDVI -0.1) NDVI<= 0.547
LAI = 3.2(NDVI) -1.08 NDVI> 0.547

Table 8 Values for use with Map 2

Col# 0: ID# Assigned to Nsoils Map
Col# 1: Saturate Volumetric Soil Moisture Content
Col# 2: Initial volumetric soil moisture content
Col# 3: Soil water tension at the wetting front (cm)
Col# 4: Soil depth (mm)

0	1	2	3	4	Units
1	0.6	0.29	3	100	blocks
2	0.6	0.29	3	300	Lacustrine deposits
3	0.54	0.29	3	300	moraines
4	0.58	0.29	3	100	screes
5	0.58	0.29	3	100	flysch
6	0.54	0.29	3	300	torrential deposits
7	0.5	0.29	3	300	weathered marls

Table 9 Values for use with Map 5

Col# 0: ID# Assigned to divi. Map					
Col# 1: Saturate Volumetric Soil Moisture Content					
Col# 2: Initial volumetric soil moisture content					
Col# 3: Soil water tension at the wetting front (cm)					
Col# 4: Soil depth (mm)					
0	1	2	3	4	Units
1	0.14	0.07	3	20	Bare
2	0.58	0.29	3	100	Forested

5.3. Methodology

5.3.1. Runoff Modelling

The rational for using LISEM to model watershed runoff was previously discussed. This subsection discusses the methodology used to model the runoff. For information on the technical hydro-modelling processes used in LISEM, readers are referred to De Roo *et al.* (1994) and Jetten (2002).

LISEM is a detailed physically based spatio-temporal model embedded in a GIS. The model incorporates hydrologic; soil erosion; and some physical influencing processes. Hydrologic processes include: rainfall; interception; surface-storage in micro depressions; infiltration; vertical movement of water in the soil; overland flow; and channel flow (De Roo *et al.* 1994). The erosion component is optional and not used here.

Figure 21 shows the methodology used in LISEM with reference to data sources. All the data used for modelling were reduced to a single gridded mask map to facilitate integration. This required all maps to be converted to the same georeference. For this purpose, all maps were converted to 10 m pixel resolution format, and georeferenced to the French national coordinate system (Nouvelle Triangulation de la France) using the Lambert III projection.

The derivative maps were created by assigning the values of table 7, table 8, and table 9 to their base maps using the command “pcrcalc –matrixtable A.map = lookupscalar (B.tbl, C, D.map)” where A.map is the derivative map required, B is the table with values, C is the column number of the table attributed to the derivative to be extracted and D.map is the base map (as shown in figure 20). In the case of table 9, the values were used to create a temporary file then used to update the derivative maps of porosity and soil moisture. DEM derivative maps and Channel maps were created using the instructions given in the LISEM manual (Jetten 2002).

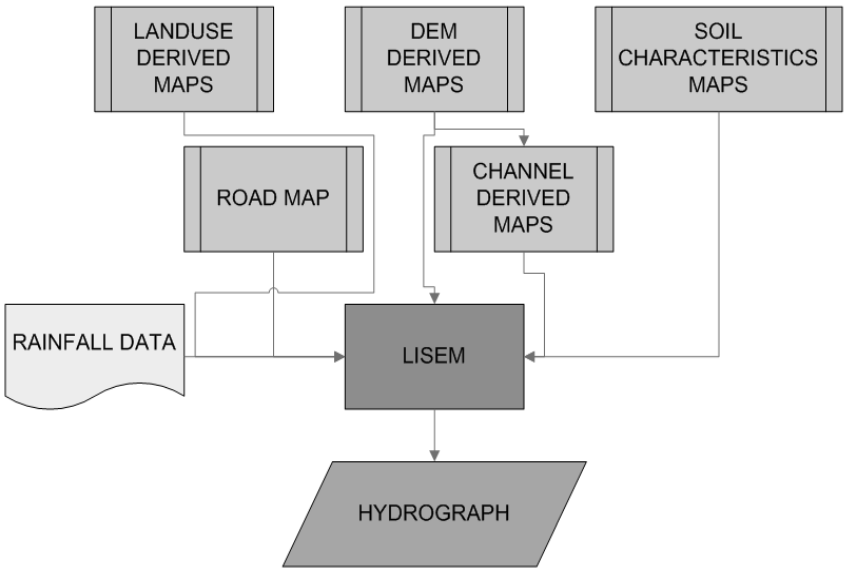

Figure 21 Rainfall-Runoff Methodology using LISEM

The lack of information on the flysch and screes slopes required the use of literature values. To find a suitable value for Ksat, porosity and initial soil moisture, a "pseudo-calibration" was done to find an appropriate set of values. To achieve this, the design approximation outlined by the SARL (2003) report was used. This consisted of a 30mm rainfall event, over a three hour period, with a total discharge of 25000 m^3. This information was used as a priori specification to calibrate the upper portion of the flysch and screes slopes. However, a distinction was made as to the area bare and the area vegetated, as shown in figure 20: Map 5. The values of bare soils given in table 7 and table 9 were chosen from the Aquifer Test Forum (ATF 2010).

As Ksat, porosity and initial soil moisture values were uncertain, a sensitivity analysis was done to understand the runoff response to their fluctuations. This involved changing Ksat values between 0.5 to 10 times the measured values, as indicated in table 8. Similarly, porosity was changed between 50 to 150% of their values, while initial soil moisture was changed to reflect the proportion to porosity as 10% and 60%. An assessment of the spatial contribution of the watershed was also done to understand the spatial distribution of rainfall within the watershed. An analysis of the spatial distribution of the rainfall, considering the area above and below 2100m elevation, as an area of geomorphologic transition.

It was difficult to associate absolute values for soil depths. The findings suggest that soil thickness measurements vary significantly. However, the evaluations were just of the top layer, and may not be representative of the second layer, which according to the mountain risk project soil thickness map vary between 2 to 4 meters. For this reason, the scenarios treated most of the soil depth as a 30cm layer as shown in table 8. For the infiltration calculation in LISEM, Green and Ampt 1 layer solution, with a permeable second layer was used.

5.3.2. Climate data analysis and storm design

The typical characteristics of storms in Faucon are not reflected in the available rainfall data for the watershed and nearby stations. In the two recent storm events of 1996 and 2003, intense rain storms caused large debris flow. The 1996 event is said to have lasted 2.5 hrs, however no rain was recorded at the climate station located on the alluvial fan (Remaitre *et al.* 2005). The 2003 storm lasted 3 hours, and also showed disparity between the expected and recorded. Regional weather radar of the 2003 event estimated 25 to 30mm, however only 13.3mm was recorded (SARL 2003) at the Barcelonnette station located 1.2 km west of the Faucon apex.

An analysis of the rainfall data for Barcelonnette climate station, between the period 1928-2004 for the months of July to October showed that a 100 year rain event consists of approximately 97mm ±15mm of rainfall. This was done using a Generalized Pareto Distribution (GPD) of the daily values, details are given in appendix II. The SARL report computed the 100 year event for various watersheds in the Barcelonnette Basin as reported in Table 10 . Among those evaluated was the Barcelonnette station. The results found that Barcelonnette 100 year return period was 90mm, using a Gumbel distribution. For consistency in comparisons, the SARL value is used in further analysis.

Table 10 100 year return period storms for watersheds in the Barcelonnette Basin - adapted from (SARL 2003)

STATION NAME	Altitude (m)	DATE OF OPERATION	DURATION OF RECORDS (years)	100yr Event (mm)
ROUSSET	675	1959	36	80
BEAUJEU	1050	1934	58	100
LE LAUZET	930	1958	15	95
LES ORRES LE MEZELET	1445	1948	47	95
ST PONS	1135	1958	15	90
BARCELONNETTE	**1135**	**1928**	**62**	90
GUILLESTRE	980	1958	15	80
COLMARS	1250	1934	41	125
VARS	1810	1936	32	105
UVERNET-FOURS	1660	1954	42	140
SAINT-PAUL	1903	1971	25	95
ENTRAUMES LE CLOT	1250	1959	36	155
JAUSIERS-LANS	1500	1961	34	90
ENTRAUNES	1250	1928	68	150
ST PAUL SUR UBAYE	1903	1959	36	90
SAINT-DALMAS	1500	1931	61	165

For design purposes, other researchers observations and perceptions regarding storms in the Barcelonnette Basin was considered. Firstly, climate variability within the basin is said to vary with elevation and slope (Weber 1994). The elevation of the Barcelonnette climate station is 1155 m, while the watershed extends to an elevation 2984m. This will also account for the disparity in rainfall measurements during the 1996 and 2003 events. Secondly, the highest rainfall intensity recorded at Barcelonnette was 30mm/hr however, other stations are said to have recorded values as high as 50mm/hr (Remaitre *et al.* 2005). Thirdly, the SARL (2003) report considers a runoff ratio of 30%, however for design purposes of extreme events Remaite *et al.* (2005) used a design intensity of 80mm/hr with a runoff ratio of 50%. Finally, while specific information on snow melt was not available, typical discharge from the Barcelonnette Basin was found to be in the order of 4 times larger than the late summer rainfall events (OMIV-EOST 2009). Based on these considerations, synthetic data was created to simulate five high intensity storm rainfall events as shown in table 11 and figure 22.

Table 11 Storm Design Intensities

Design Storm (mm)	1st hour intensity (mm/hr)	2nd hour intensity mm/hr	3rd hour intensity (mm/hr)
30	7.5	15	7.5
90	20	50	20
90	30	30	30
150	50	50	50
160	80	80	0

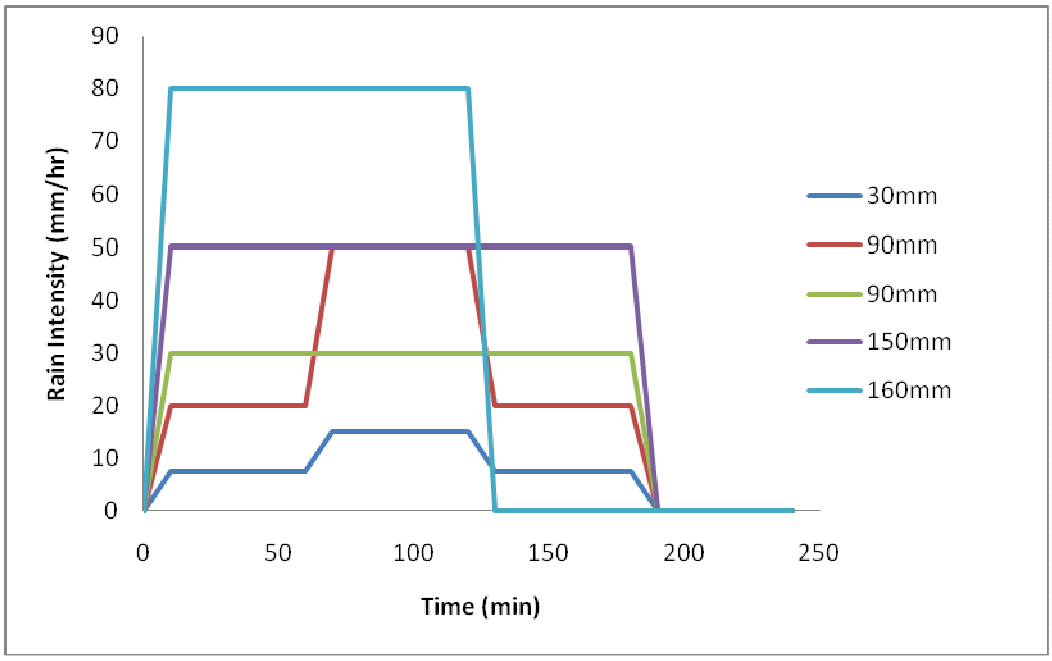

Figure 22 Design Rainfall Events

5.4. Results

The result of the calibration, as shown in Figure 23, was determined with Ksat and porosity of 3 mm/hr and 14% respectively. The results also show a rainfall to runoff ratio of 13%, which was much lower than the design value of 30% used in the SARL report.

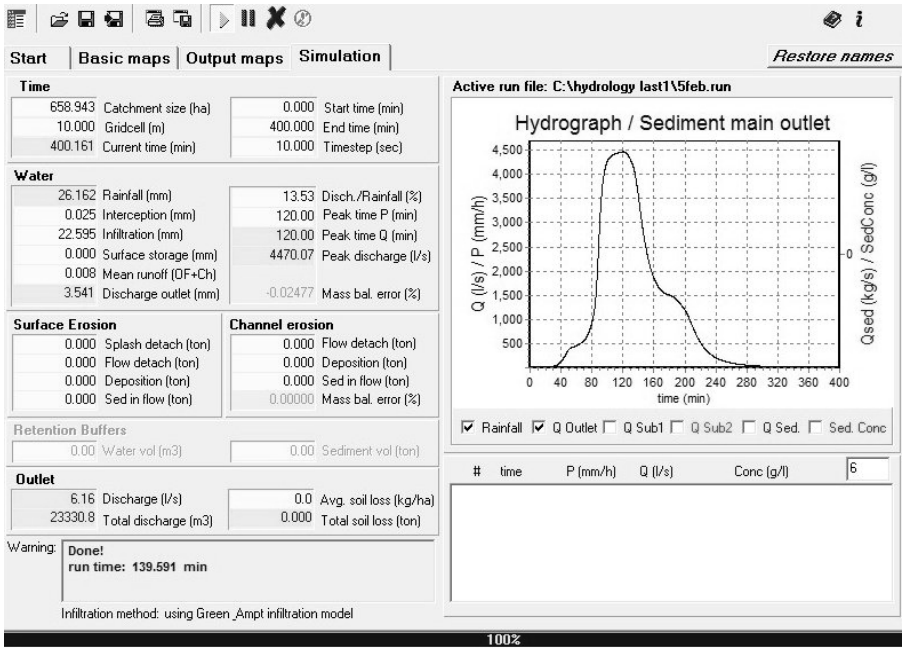

Figure 23 Pseudo calibration results

The results of the Ksat sensitivity is presented in table 12 and figure 24 . Values of 0.5–0.75 (50%-75%) Ksat, correspond to the lower values measured. Values of 5-10 are in the order of the larger ring and pF ring measurements. The results show a large distinction when infiltration is halved.

Table 12 Design for Ksat sensitivity based on 50mm/hr for 3 hours storm event. Considering only the region less than 2100m

Variable %	Discharge (m^3/s)	Peak (m^3/s)
50	164724.7	20
75	92418.74	9.73
100 (as is)	74186.6	7.85
125	63838.71	6.12
150	61757.51	5.93
200	58496.84	5.62
500	45603.5	4.41
1000	33810.3	3.17

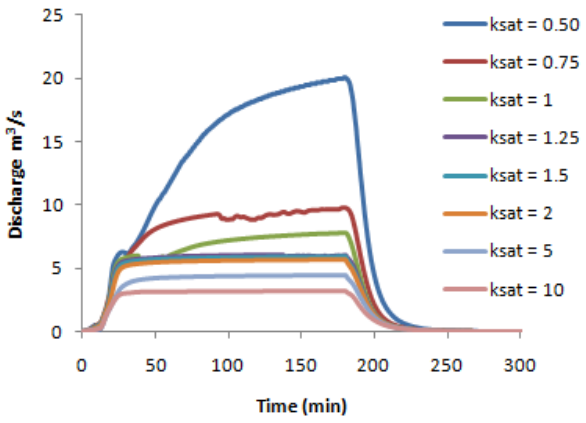

Figure 24 Rainfall/runoff sensitivity to Ksat

The results shown in table 13and table 14, figure 25 and figure 26, shows little sensitivity to changes in porosity and soil moisture. During these runs, where soil moisture was larger than the porosity, a value of 50% of the porosity was used as the soil moisture. The results show little differences.

Table 13 Design conditions and results for porosity testing

Variable	Discharge (m^3/s)	Peak (m^3/s)
50%	236505	25.5
75%	237661	24.6
100% as is	226106	23.8
125%	217851.2	23.138
150%	211467	22.5

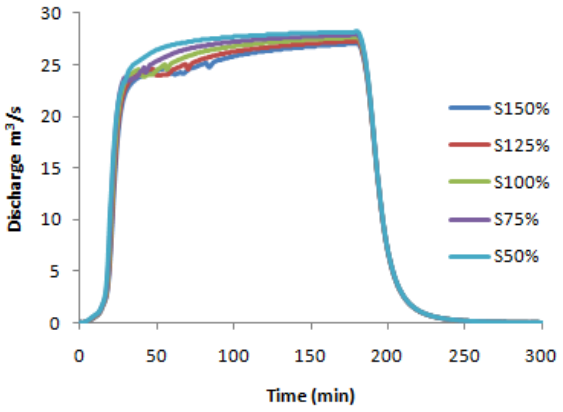

Figure 25 Runoff sensitivity to porosity

Table 14 Design conditions and results for soil moisture testing

Variable	Discharge (m^3/s)	Peak (m^3/s)
0.10	272925.7	27.3
0.29 (as is)	277399	27.6
0.60	286491.7	28.1

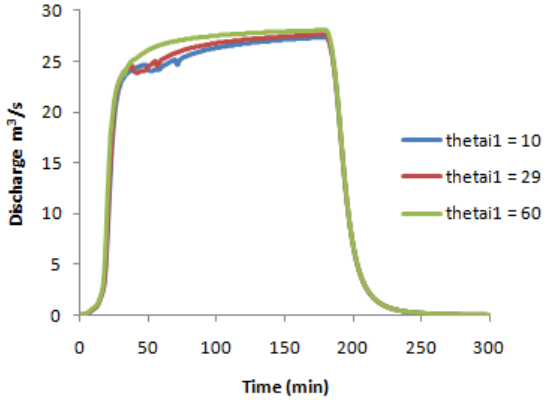

Figure 26 Runoff sensitivity to initial soil moisture

The differences in rainfall spatial distribution contribution within the watershed is given in table 15 and illustrated in figure 27.The results indicate that the upper watershed contributes to most of the runoff, however as the intensity increases, the percentage contribution decreases. Also notable, is the event duration is maintained more by the upper watershed. In contrast the lower part of the watershed, has a more define peak, but with shorter duration.

Finally, table 16 and represent the various storm designs corresponding to figure 28. The results show high peaks for high intensities. Likewise duration of the peak is relatively flat and also response to the design input intensities. However, the 160 event did not respond with a flat peak.

Table 15 Design for Spatial Sensitivity

Variable	Discharge (m^3/s)	Peak (m^3/s)
R30	22858.75	4.38319
R30>2100m	15192.96	2.99001
R30<2100m	5598.603	0.831749
R150	238074.5	24.075
R150>2100m	105722.1	9.99009
R150<2100m	47975.6	5.36387
R30	22858.75	4.38319

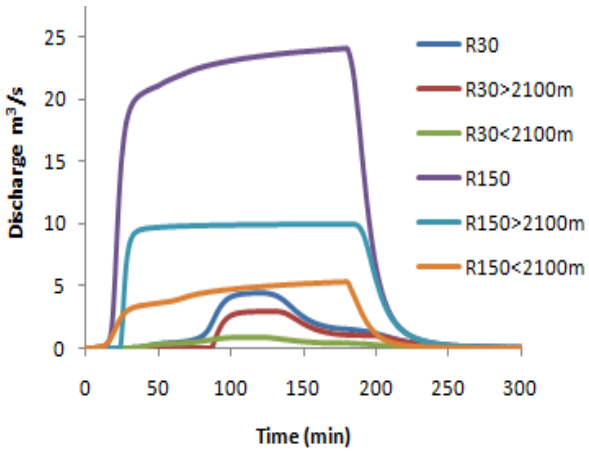

Figure 27 Spatial sensitivity of rainfall/runoff

Table 16 Sensitivity of watershed to different storm designs

Event (mm)	Intensities (mm/hr)	Discharge (m^3/s)	Peak (m^3/s)
30	7.5 - 15 - 7.5	23275.5	5.1
90	20 - 50 - 20	143584.2	26.6
90	30 - 30 - 30	142138.8	14.2
150	50 - 50 - 50	277399.0	27.6
160	80 - 80	348877.5	54.7

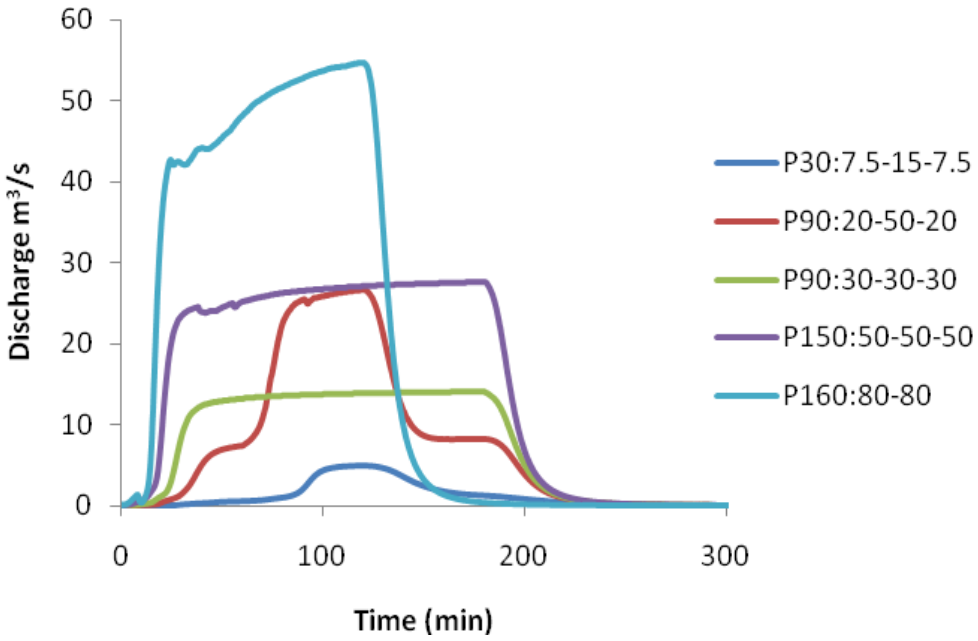

Figure 28 Runoff sensitivity to rainfall

6. Hydrodynamic Flood Modelling

6.1. Introduction

This section models the hydrodynamic flow of water on the alluvial fan for different scenarios. The scenarios chosen are not exclusive and only reflect some of the key uncertainty in data and boundary conditions. These conditions include: storm design; infiltration; blockage location and DTM sensitivity. The 50-50-50 mm/hr intensity, 150mm rainfall storm design, as shown in figure 29, was used as the 100 year event,

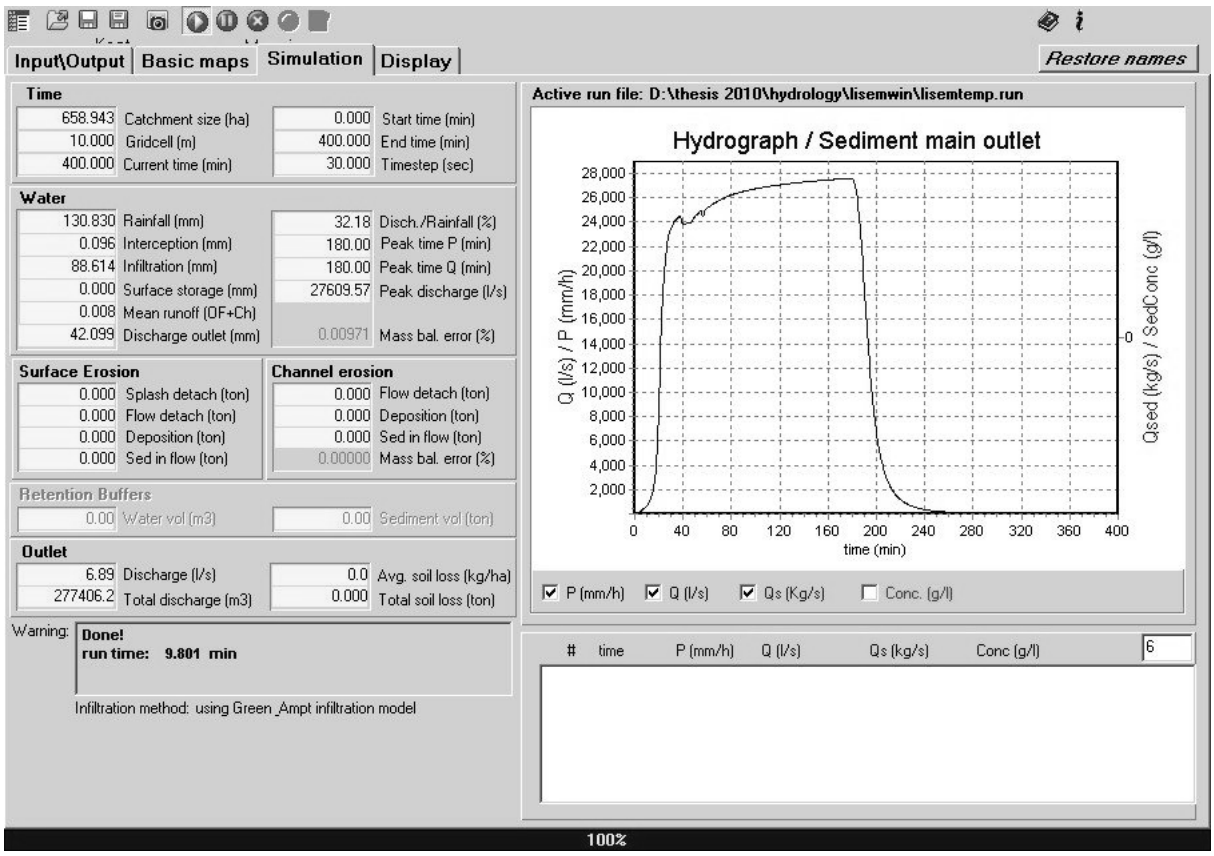

Figure 29 Hydrograph for 150mm storm event

The source of flooding on an alluvial fan is attributed to the inability of the channel to transport its fluvial contents either in the form of water or debris flow. This required an evaluation of the conditions at which the flow capacity of the river fails. Either due to high storm discharge or combinations of infilling and blockages. Blockage susceptibility was evaluated based on the conditions outlines earlier: slope, and past deposits.

6.2. Methodology

6.2.1. Blockages

To understand the effects of flooding, infilling and blockages the methodology shown in figure 30 is used. If no flooding was evident from the event, then the 2003 debris flow blockage was introduced. If there was no substantial flooding, then an infilling scenario was included. Thereafter, once substantial flooding occurs, the boundary conditions including DTM inaccuracies is evaluated.

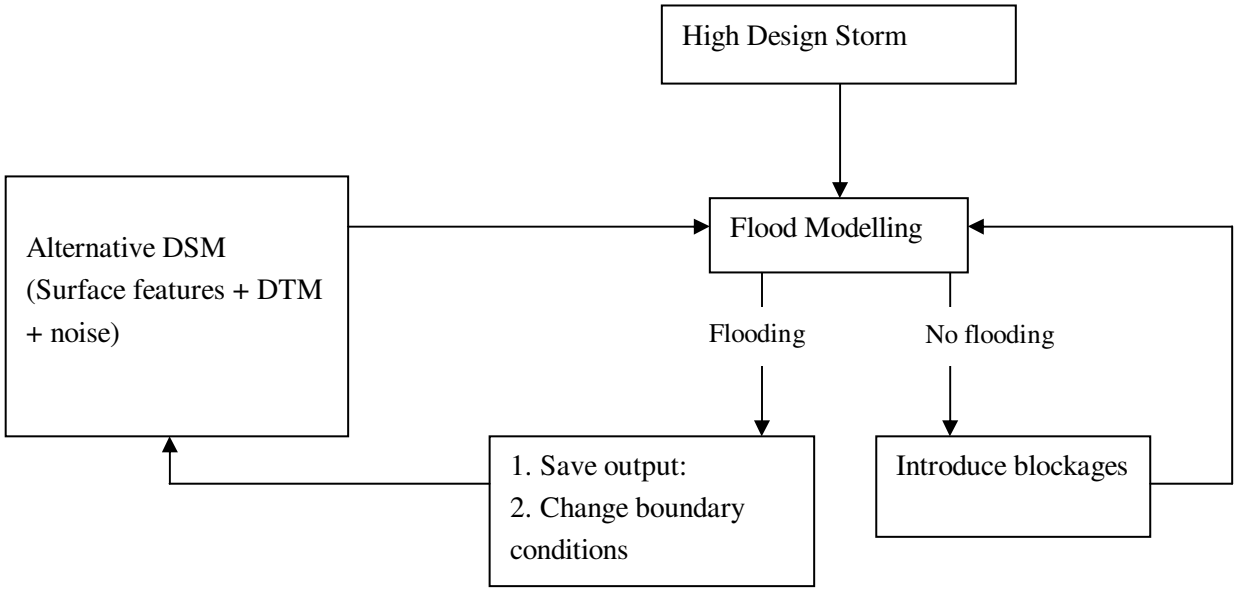

Figure 30 Flooding Scenario Methodology

6.2.2. Flood Modelling

The processing of data and generation of flood models was done in Sobek 1D2D. The data, conditions and methodology used in Sobek is shown in figure 31. The model required the DSM which was made by merging the DTM and surface expressions such as buildings. The 1D channel was defined using the river map and cross sections data. However, during the infilling scenario, the 1D channel failed, and the channel, dikes and alluvial fan had to be treated as a 2D flow problem.

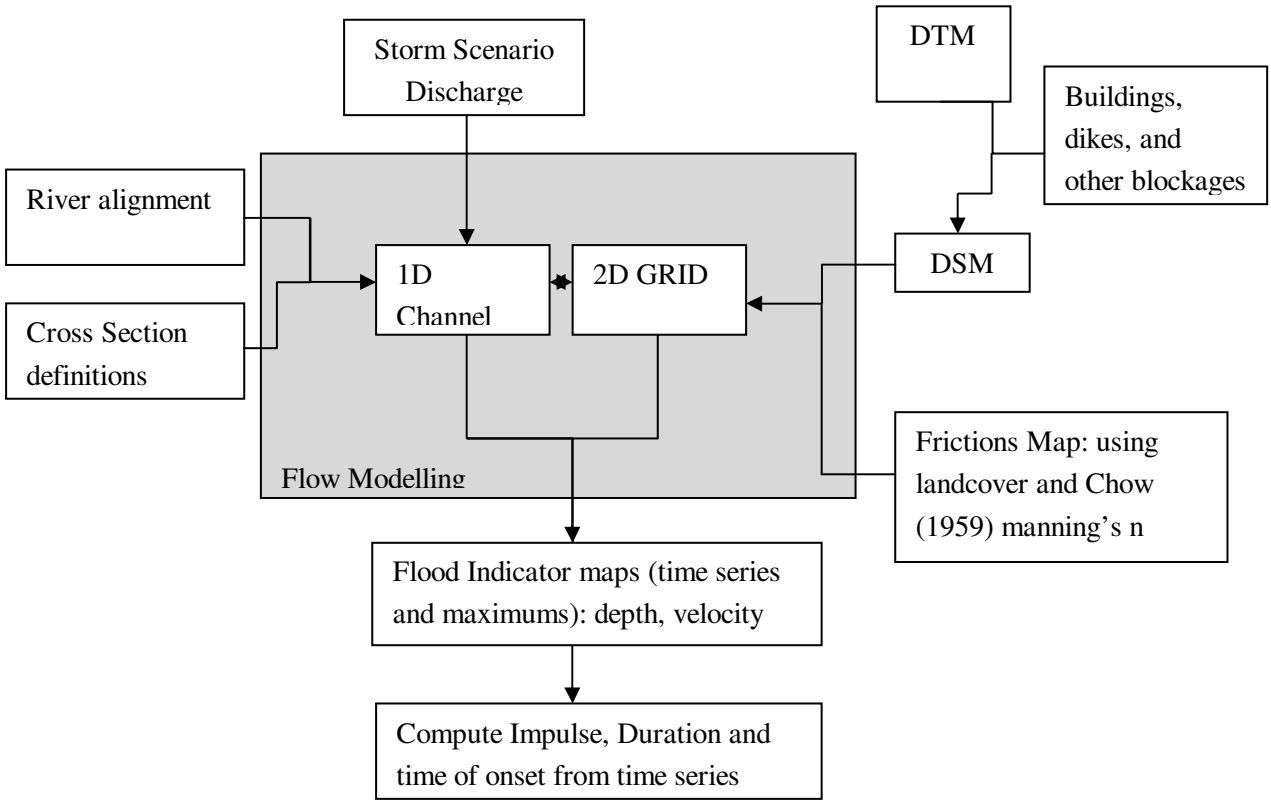

Figure 31 Flood modelling methodology using Sobek

The ID2D model used in Sobek was done by a flow node, five cross section nodes, three bridge node and the schematization of the river. This model is shown in figure 32. Also shown, are the cross sections of the river and bridges. As mentioned earlier the DSM was used along with a roughness map based on the values used in the runoff modelling.

In order to simulate the DSM without a 1D channel, the DTM had to be modified. This was done to express the river and dikes. The modification was based on making a channel and dike masks from the cross section information and the secondary channel survey information gathered during the field work. The process involved burning the river into the DTM and adding the dikes using the masks. Likewise the DTM was modified to include the Ubaye River with a gentle downward slope to Barcelonnette. With each scenario, the channel mask was modified to the simulated level of infilling.

Without a 1D channel the flow model, using the flow node did not work. To force the 2D scenario, the channel flow conditions in Sobek were manipulated. This was done with a dummy channel. The channel used a 1D flow boundary node, which defined the discharge, connected to a storage node as shown in figure 33. The storage node, in effect a storage pit, was set to be shallow with a small capacity. This design allowed water to flow out of the dummy 1D channel and into the 2D channel, when the pit was full. The pit specification used was $10m^3$ of storage with a depth of 1m.

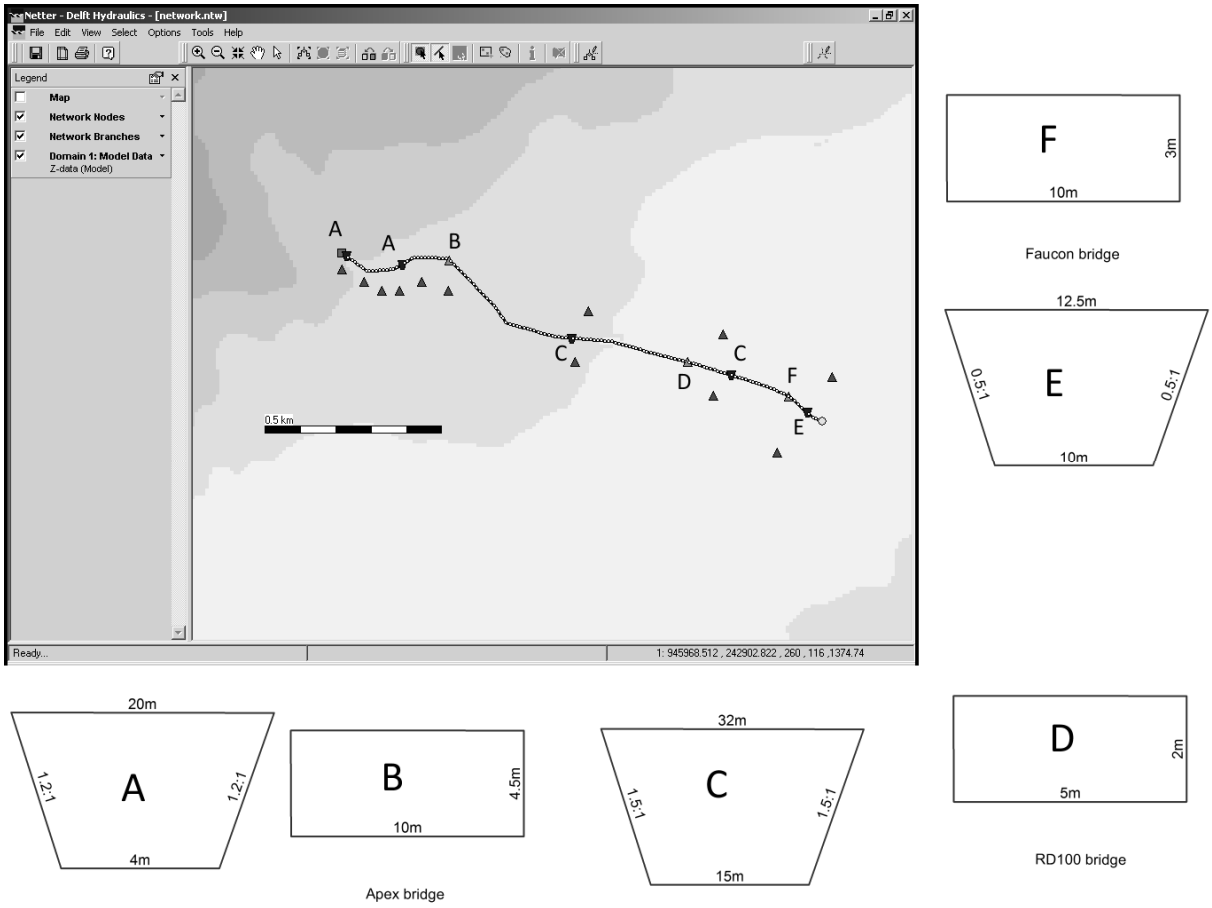

Figure 32 Initial model in Sobek, without infill or blockages

As mentioned by Hamilton *et al.* (1988), the most important component for alluvial fan flooding is the impulse. Sobek output maps were in the form of 5-minutes time series maps of depth and velocity saved as an ascii format. To obtain the maximum impulse of the flood on the alluvial fan, each time series pair of maps (depth and velocity) was first converted to an impulse map. Thereafter the maximum impulse was extracted from amongst the created impulse map, on a pixel by pixel basis. This was done using a small program in Scilab. A copy of the program is included in appendix III.

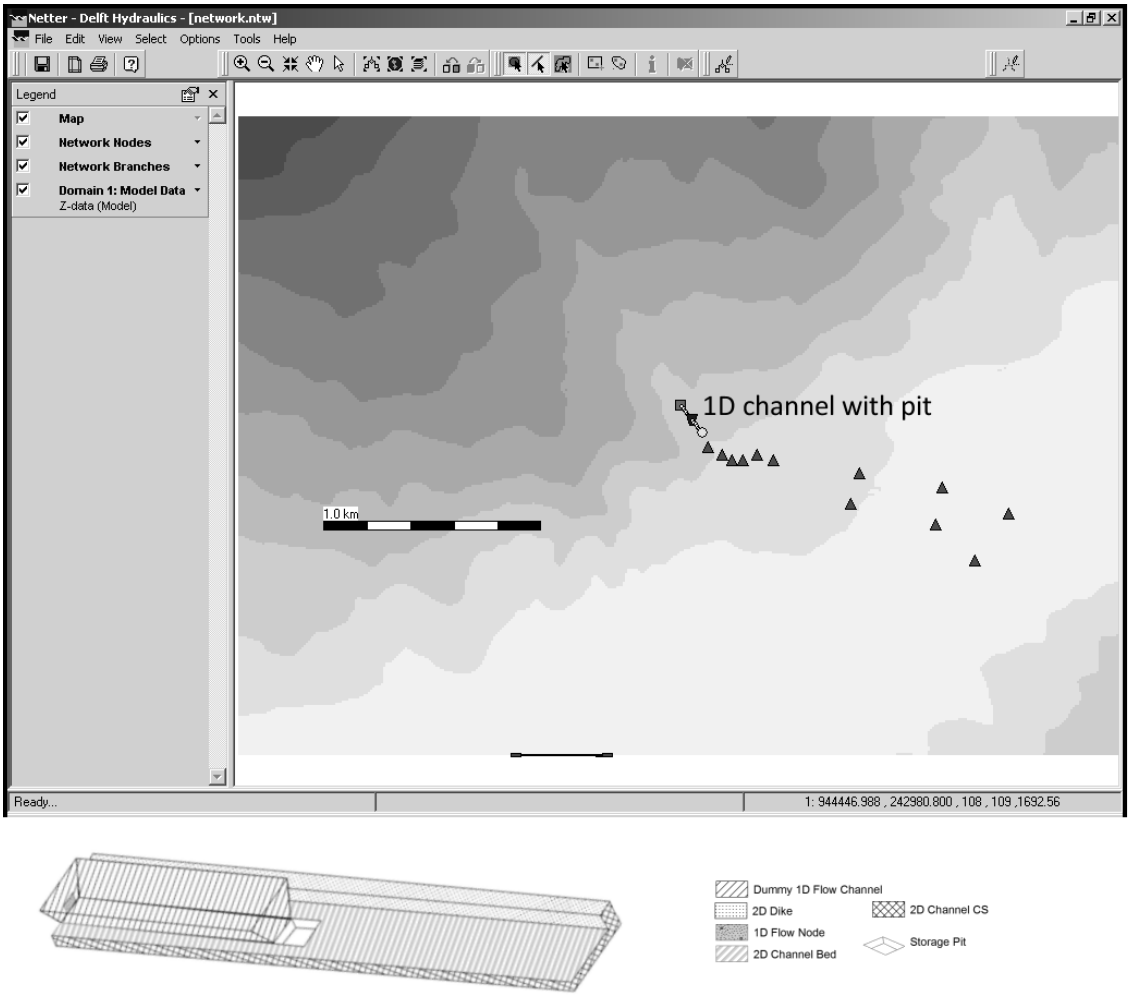

Figure 33 Forced 2D conditions for scenario modelling

6.2.3. DTM Sensitivity

As discussed in chapter 2, the terrain changes that occur during a flood scenario with mud or debris may change the terrain with depositions and erosion. Also the effects of DEM sensitivity to inaccuracies and resolution were discussed. Considering that on an alluvial fan, the gradient of slope changes in a DEM should be more significant than flatter terrain, the sensitivity of DEM sensitivity was chosen for testing.

In this process DEM sensitivity is considered in the context of DTM sensitivity, problems with the terrain modelling. One such problem is the accuracy of the elevation data, and the subsequent inaccuracy representation in the DTM. To access such an error, the study used the method designed by Hunter and Goodchild (1994; 1997) which adds spatially auto correlated noise based on (eq 6.1):

$$e = \rho We + N(0,1) \qquad (6.1)$$

Where e represents the grid value matrix, ρ is a parameter function (ρ=0.002/3), W is a weight matrix to maintain autocorrelation and $N(0,1)$, is a normal distributed random matrix. Although the W matrix is referred to as weight matrix, it is used as a binary mask, to focus on the area of evaluation. Scaling of the e matrix is achieved by the ρ parameter. The N matrix is the error matrix having a normal distribution, with standard deviation 1m. 1m was chosen, based on similar work by Zerger *et al*. (2002) who found an general accuracy of 2m using a 20m DEM resolution, that was obtained from a 1:25000 map.

In the generation of the error for the DTM, the original grid DTM values are used in the first instance as e, thereafter it is iterated until a defined threshold standard deviation value of 10% difference is obtained. For comparison, non-spatially correlated noise was also added to the some scenarios. Scilab program included in appendix III.

6.2.4. Visualization and Digitizing

For the purposes of visualization, results were smoothened to obtain a clear depiction of events. This was done through the application of a 3×3 smoothening filter and classification through value ranges. Using the smoothed images, the flow paths were more distinguishable to ease digitizing as shown in figure 34. Concentrated flow lines were drawn as primary, secondary or tertiary based on their impulse intensity and their order relative to the flooded apex.

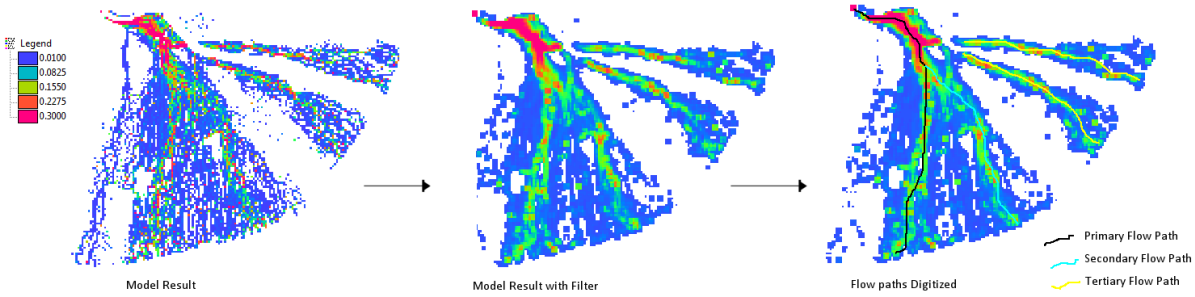

Figure 34 Improving the visual conditions of the maps to facilitate digitizing

6.2.5. Parameterization

The two blockage conditions tested included: angles of 2 degrees or less and past events/indicators. The first condition was found unsuitable in the study area. With an average slope of 8 degrees, the river is not susceptible to blockage from the first condition. The second condition, while some flooding occurred, was relatively minor, occurring around the RD100 bridge. The bridge was completely blocked during the 2003 event. As such the effect of infilling and its primitive blocked point (apex) were also considered in the analysis. Table 17 shows the design parameters used for the generation of the results.

Table 17 Scenarios design information

Map #	Debris	Infilling	Error – matrix	Remarks
1	X	X	X	No flooding (150mm)
2	2003	0	X	(150mm Storm event)
3	2003	1m	X	(150mm)
4	2003	2m	X	(150mm)
5	2003	2m	N(0,1.5) – R	(150mm)
6	2003	2m	N(0,1.5) – R	(150mm)
7	2003	2m	N(0,1.5) – R	(150mm)
8	2003	2m	N(0,0.5) – R	(150mm)
9	2003	2m	N(0,0.5) – R	(150mm)
10	2003	2m	N(0,0.5) – R	(150mm)
11	2003	2m	N(0,0.5) – R	No buildings (150mm)
12	2003	2m	N(0,0.5) – R	(150mm)
13	2003	2m	X	No buildings(150mm)
14	2003	2m	N(0,0.5) – S	(150mm)
15	2003	2m	N(0,0.5) – S	(150mm)
16	2003	2m	N(0,0.5) – S	(150mm)
17	2003	2m	N(0,0.5) – S	(150mm)
18	2003	2m	N(0,1) – S	(150mm)
19	2003	2m	N(0,1) – S	(150mm)
20	2003	2m	N(0,1) -R	(150mm)
21	2003	2m	N(0,1) -R	(150mm)
22	2003	2m	X	160mm storm event
23	2003	2m	N(0,1) -R	(160mm)
24	2003	2m	N(0,1) -R	(160mm)
			-R Random Matrix (Normal Distribution)	
			-S Spatially correlated Random Matrix (Normal Distribution)	

6.3. Results

The maps presented below in figure 35 and figure 36 consists of the resulting maps based on the scenarios of table 17, all maps are as unfiltered. However, flooding in the Faucon and Ubaye rivers were masked. The results show that under conditions of no blockage, no flooding occurs (Map 1). Map 2 and Map 3, shows the flooding with the 2003 debris blockage and some infilling. The infilling conditions of Map 4, was used for the remaining of the testing as it was considered significant, and suitable for testing the effects of the DTM uncertainty. The smooth effect of Maps 4, 13 and 22 is attributed to the absence of DTM noise that is included in the other maps. However, Map 11 also showed a smooth effect, yet it did have noise.

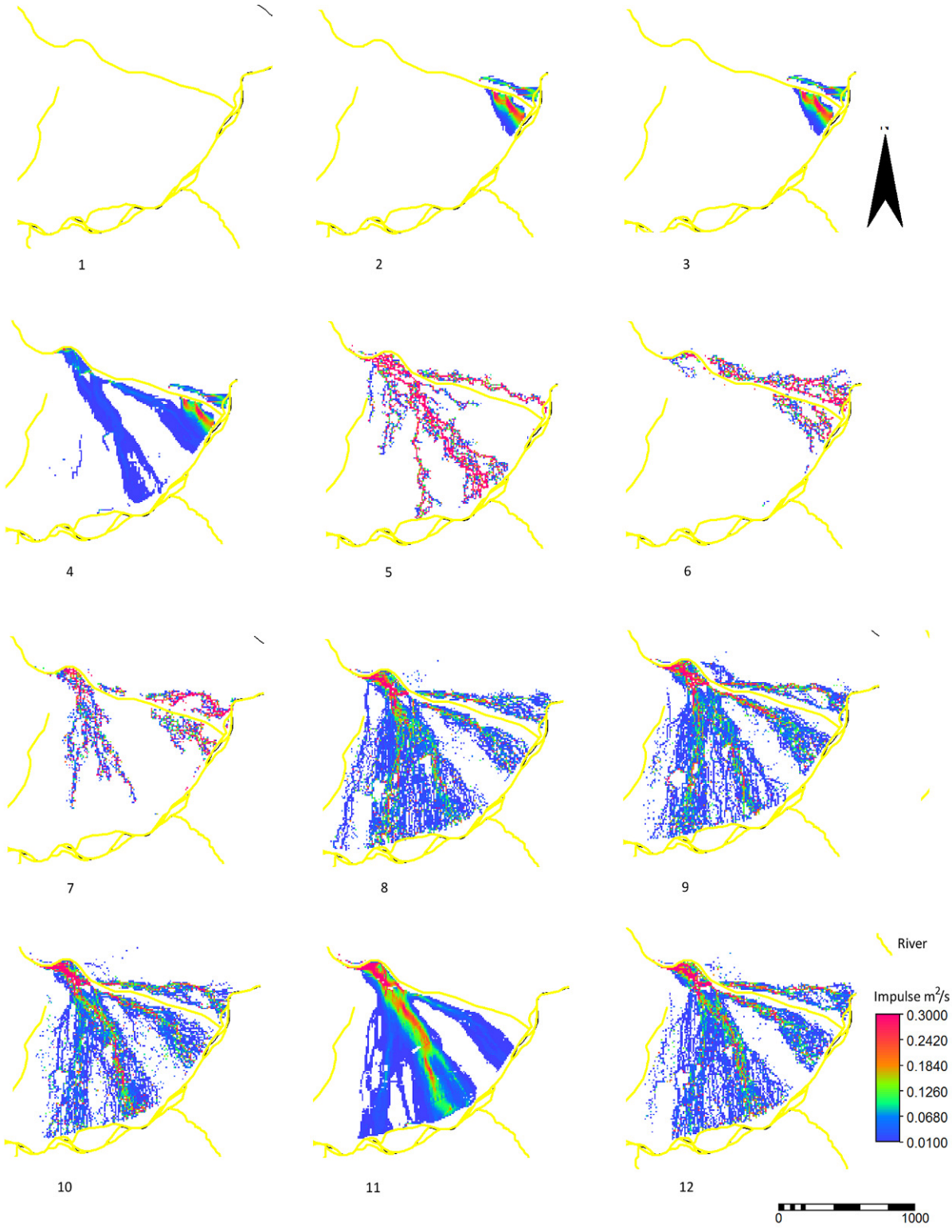

Figure 35 Results of scenarios 1 to 12

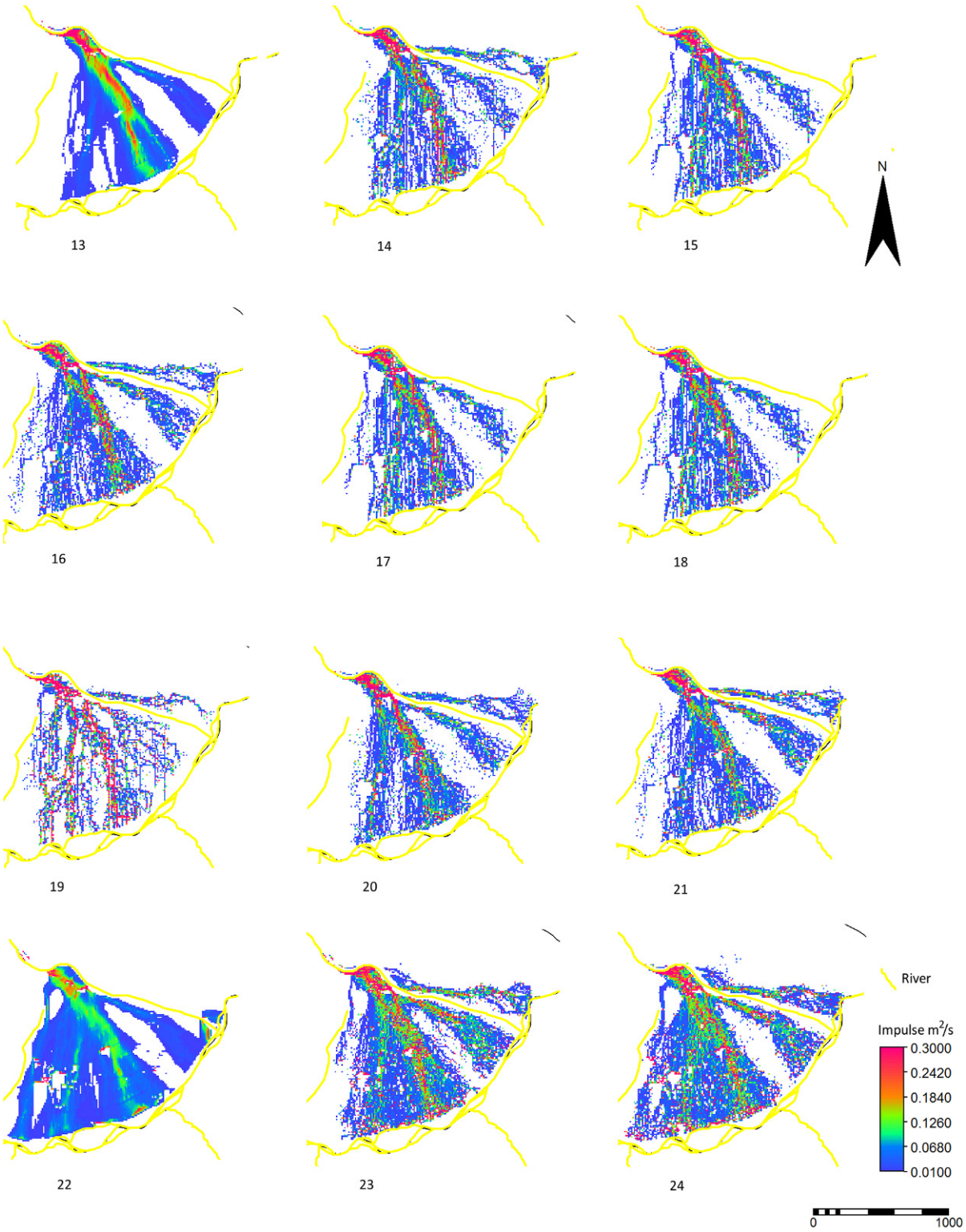

Figure 36 Results of scenarios 13 to 24

The concentrated flow paths were digitized as explained in section 6.2.4, the results of which is represented in figure 37 and figure 38. The aggregated flow paths show a high concentration in an almost straight line from the watershed channel and apex to the centre of the alluvial fan. When the results are broken into spatially correlated and non-spatially correlated noise, a systematic pattern emerges for the former, and a non-systematic pattern in the latter set.

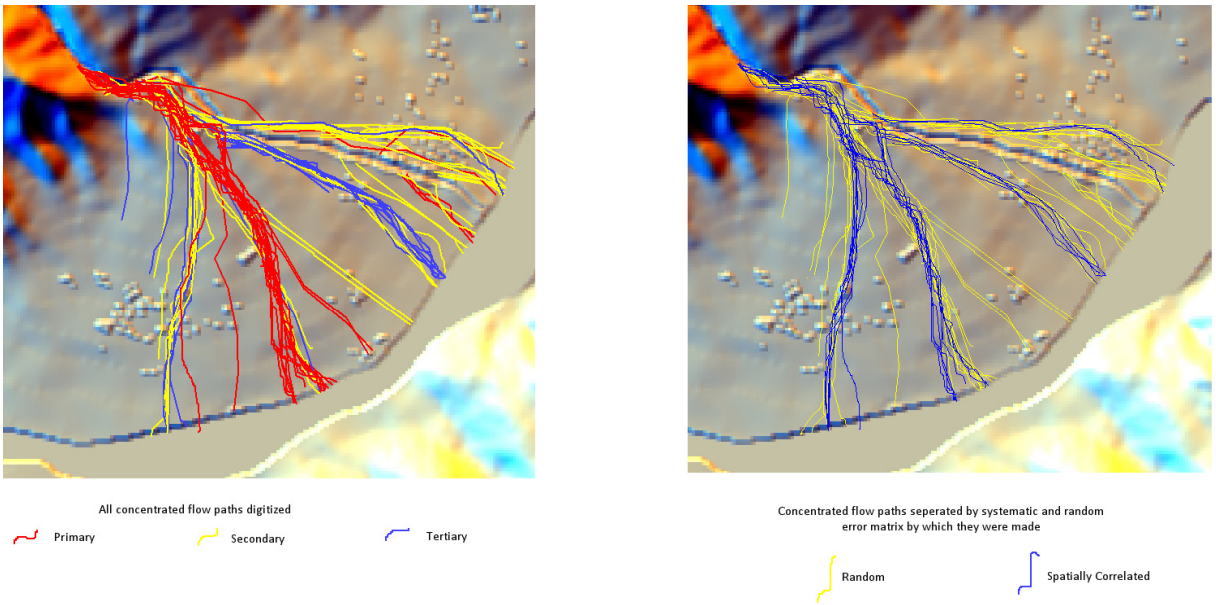

Figure 37 Mapping of concentrated flow paths by impulse strength (left image) and by the DTM noise added (right image)

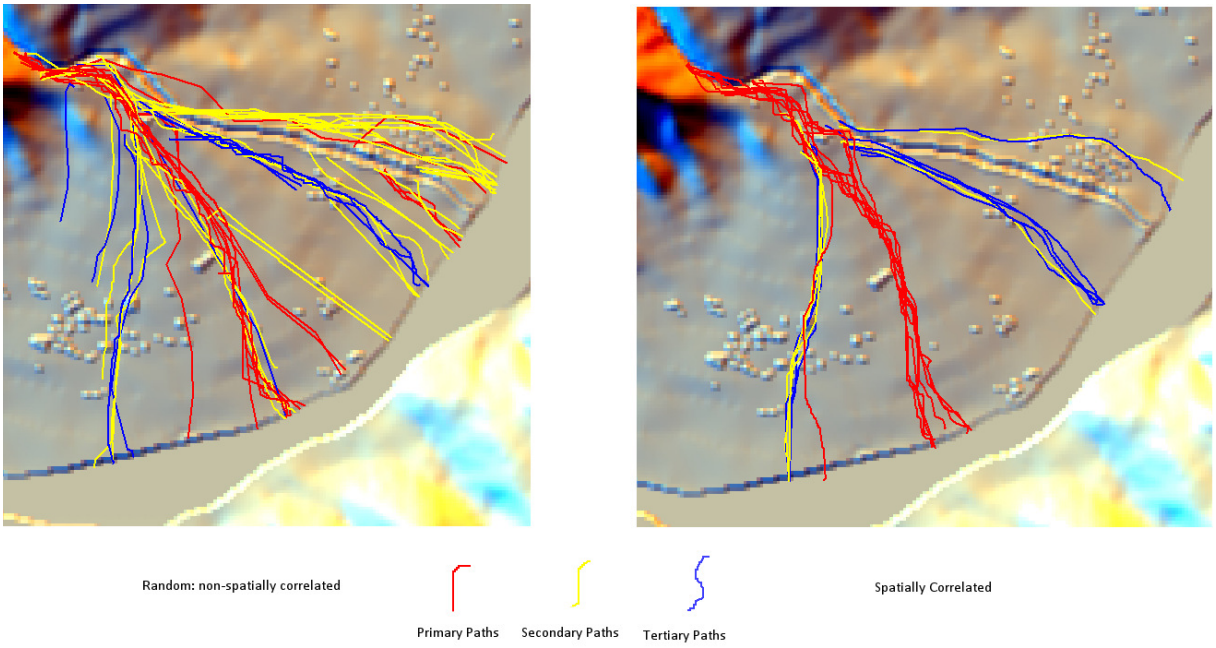

Figure 38 Mapping of concentrated flow paths by random non-spatially correlated noise (left image) and by random spatially correlated noise (right image)

7. Discussion

7.1. Data collected and Analyzed

Acquiring soil properties for modelling proved difficult. Firstly, the Ksat values was based on assumption that the small ring results were accurate. However, the method is untested and unverified, and may seem more wishful than actual. By reducing the results to methods, the sampling sizes were too small to give a true assessment. In can also be argued that the small rings readings were too homogenous and did not represent the general conditions of the surface. However, the reverse argument may also be possible. All three methods had the same median value for the pasture areas, which predominantly had signs of sealing. However, in the grassed and forested areas, pF rings and the larger rings were difficult to penetrate the subsurface because of dense root layers. In fact the small rings were the only method to have least disturbed the surface and not be influenced by the subsurface. In general the pF rings and the large rings are unsuitable for the environment.

Another problem of concern was the addition of water during sampling and the transport of saturated samples. It became evident that some of the saturated sampled became compacted after transport. The effect of compaction would explain the high RMS between sampling measured pseudo-lab and using the permeameter, with the later generally having a lesser infiltration rate. Similarly, although not explored it would have also affected the porosity values. The saturated samples were also unsuitable for use in measuring the soil moisture content at analysis. Although only the unsaturated samples were used, there were large differences in values which can be attributed to the moistening in the field, which at times, required soaking the ground.

Soil depth samples were also not well determined. Although some effort was made to understand the processes, it was difficult to ascertain suitable values for use in LISEM, primary because the model chosen was based on a one layer Green and Amp model. However field observations suggested that a two layer approach is more suitable for this site. In addition, the soil thickness information obtained (Remaitre 2006; 2009), suggests that the thickness of the moraines are between 2-4 meters. Van *et al*. (1997) found that in the Terres Noires Region of Barcelonnette, the second layer was 1.5m below the surface. For these reasons, it was felt that the use of small depths for soil thickness may be underestimating the processes occurring in the first and second soil layers.

7.2. Runoff Modelling

The results of the runoff modelling showed that the expected 100 year storm based on Barcelonnette's data, is significantly different than the 100 year event from other wetter watersheds in the same basin. The 90mm 100 year event for Barcelonnette was found to be half of the discharge of the design 150 mm storm event. Under conditions of the same peak intensity, both can have the same peak discharge, however the duration would be shorter with the smaller 90mm event. It is important to note that while 50mm/hr is used as a design intensity based on the maximum recorded at other watershed, the maximum recorded at Barcelonnette was only 30mm/hr.

Also used was a 2 hour 160mm storm design event. It is interesting to note the deviated from the norm of other events in that its first runoff peak responded with intensity as the other did, however it had a further peak during its second hour. This may be attributed to the rainfall intensity being faster than the infiltration rate.

It was also interesting to note that the porosity and soil moisture had little response to runoff. However, Ksat had a range that deviated by about 5 m^3/s from the assumed base conditions of median small ring values. However, if the Ksat value is half of base values, the difference is about 12 m^3/s more discharge.

The results also showed that the spatial distribution can greatly affect the runoff, with the most runoff coming from the head of the watershed. This is understandable since the head material is mainly calcitic limestone, which has lower Ksat and porosity values.

7.3. Flood Modelling

The results showed that even with a "extreme" 150mm storm event, which is greater than a 500yr safety level, based on Barcelonnette data, no flooding will occur. However, if the event is accompanied by blockages or occurs after blockages, can lead to flooding. The modelled infilling based on the 2003 event modelled only 65000 m^3 of blockage, while the amount of debris removed was about 70000 m^3. The increase of 2m to the 2003 event consisted of 120000 m^3 total infill. Empirical models of the 2003 event by SARL (2003), gave the range of debris between 75000-15000 m^3. As such, the scenario is within the modelled limits, but on the higher side. However, the context of modelling the channel within the 2D space can under-estimate or over-estimate the volume of the channel, as the raster 2D environment used was 10m resolution the river was treated as a box-shape, but in reality it has a trapezium form along the alluvial fan.

During modelling, features on the alluvial fan were not well represented in the models. This was associated with two problems. Firstly, the terrain was not well represented in the DTM. Features such as roads were cut into the terrain with differences of 2 meters in some areas. Also, the terrain was not as smooth as the DTM suggests, rather there were areas with vertical drops of 12 meters and large saddle agricultural fields and terraces that would act as retention ponds in the event of such a flood. Secondly,

the merging of small features such as walls and 2.5m roads, into the DTM was not feasible because of the resolution of the DTM and feature sizes.

The results of the flood models showed that a small error of 1m, applied using a normal distribution can have a significant effect on concentrated flood paths. However, the correlation of the error (noise) greatly affected the results. Models using spatially correlated noise tended to have systematic flow paths concentrated at the toe of the alluvial fan. However, random noise, not correlated, showed non-systematic flow paths. Such non-systematic paths are similar to the experimental model by Weaver as shown in figure 5 (Schumm *et al.* 1987).

Adding spatially correlated noise was based on the recommendations of (Hunter, G. J. and Goodchild 1994; 1997; Zerger *et al.* 2002). The rational is that points that are close to each other should have similar errors. However, it is key to note that the evaluation is based on similar errors of nearby points, however in alluvial fan flooding the deposition of debris flow may is random. The random deposition was the rational for defining "unpredictable flow paths", as stated by the NRC (1996). This therefore shows that the type of noise added must take the source of uncertainty attempted to be simulated. In circumstances where the uncertainty is from DTM inaccuracies, then spatial correlated noise may be better, however when the uncertainty is random, such as in flow deposits, then random non-spatial noise is perhaps better.

8. Conclusion and Recommendations

8.1. Conclusion

The study sought to investigate a number of questions relating to the objective of DTM uncertainty, the following are the questions researched and the conclusions drawn:

What is the influence of infiltration and water storage parameters on the runoff?
Does the hydrograph represent typical flood inducing storm events?

The study found that while infiltration is significant the effects of spatial distribution and rainfall intensity is more important. Porosity and soil moisture content seems to have little influence on the discharge. The influence of soil depth remains uncertain and requires further investigation.

Rain events in Barcelonnette does not represent past events in the Faucon watershed. As such, hydrograph for a 100 year event made with data from Barcelonnette does not seem to represent storm conditions experienced in Faucon.

Can flooding occur during a 100 year event without blockages or infilling?
Which areas on the channel are sensitive to breaching in the event of infilling?
Which areas on the alluvial fan are sensitive to flooding?

The results showed that during an event larger than the 100 year Barcelonnette storm, there was no flooding in the absence of infilling. During infilling, the results showed that the region surrounding the lowest bridge (RD100) is particularly vulnerable. However, with a larger quantity of infilling, the channel at the apex becomes sensitive to breaching. During such a breach, most of the alluvial fan, on both sides of the torrent is vulnerable to flooding.

How sensitive is modelled overland flow to terrain inaccuracies?
Where on the alluvial fan is there risk of high impulse?

Overland flow was found to be particularly sensitivity to terrain inaccuracies. However the sensitivity reflects the modelled uncertainty. Spatially correlated uncertainty gave areas with concentrated high impulses, the results reflected a systematic response. Uncorrelated noise, resulted in unsystematic flow expressions along the alluvial fan. However the latter follows the expected behaviour of alluvial fan flooding.

8.2. Recommendations

- A more detailed study of Faucon is required. The findings of this report should be used as guide for future research. Certainly, a good soil depth investigation is required along with infiltration. A comparison study of methods using the inverse bore hole method and disk infiltrometer, along with the methods used in this study is worth further investigation. The study of infiltration should also be extended to the second sublayer, along with an appropriate model, such as the Green and Ampt 2 layer model.

- The relation between past landuses and soil properties may also be interesting, along with a study of geomorphology relationships.

- Discharge data should be obtained to calibrate the runoff model. However, calibration during low rainfall events may be unsuitable because of the irrigation practices that exist. These practices divert water from the main channel, which can be significant if calibrating during low runoff events. In addition, it was apparent that the infiltration in the channel may be significant, another item that warrants additional research. As any further study measuring the flow of the excess diverted water may prove useful to calibration.

- A higher accuracy DSM, perhaps LIDAR, should be used to validate the findings of this study regarding flow paths and inundations, caused by DTM inaccuracies.

- The effect of object blockages, such as building, on the concentrated flow paths requires a fine DSM of higher accuracy, perhaps LIDAR.

- Finally, the effect of DTM uncertainty should be further tested on different terrain surfaces, along with the type of uncertainty (spatially correlated or not) and the conditions causing uncertainty and their effects on flood modelling.

9. References

Alkema, D. (2003). Flood risk assessment for EIA : environmental impact assessment, an example of a motorway near Trento, Italy. In: Studi Trentini di Scienze Naturali : Acta Geologica, 78(2003), pp. 147-154.

Alkema, D. (2009). Ksat Test. Fieldwork Instructions, Faculty of Geo-Information Science and Earth Observation. University of Twente.

Arhonditsis, G., C. Giourga, et al. (2002). Quantitative assessment of agricultural runoff and soil erosion using mathematical modeling: applications in the Mediterranean region. Environmental Management 30(3): 434-53.

ATF. (2010, 28 January 2008). Aquifer Properties. Aquifer Test Forum HydroSOLVE, Inc. Retrieved January 12, 2010, from http://www.aquifertest.com/forum/properties.htm.

Bello, M., J. Lopez, et al. (2003). Simulation of flooding and debris flow in the Cerro Grande River Acta Cientifica Venezolana 54(1): 11.

Beven, K. J. (2001). Rainfall - runoff modelling : The primer. Chichester, West Sussex, John Wiley & Sons.

Bharati, L., K. H. Lee, et al. (2002). Soil-water infiltration under crops, pasture, and established riparian buffer in Midwestern USA. Agroforestry Systems 56(3): 249-257.

Blair, T. C. and J. G. McPherson (2009). Processes and forms of alluvial fans. Geomorphology of Desert Environments**:** 413-467.

Bronstert, A., B. Glusing, et al. (1998). Physically-based hydrological modelling on the hillslope and micro-catchment scale: examples of capabilities and limitations. IAHS publication. 248: 207.

Bronstert, A. and E. J. Plate (1997). Modelling of runoff generation and soil moisture dynamics for hillslopes and micro-catchments. Journal of Hydrology 198(1-4): 177-195.

Carrivick, J. L. (2006). Application of 2D hydrodynamic modelling to high-magnitude outburst floods: An example from Kverkfjöll, Iceland. Journal of Hydrology 321(1-4): 187-199.

Chow, V. T. (1959). Open channel hydraulics. Tokyo, McGraw-Hill.

Clarke, L., T. A. Quine, et al. (2009). An experimental investigation of autogenic behaviour during alluvial fan evolution. Geomorphology In Press, Accepted Manuscript.

Clarke, R. T. (2008). A critique of present procedures used to compare performance of rainfall-runoff models. Journal of Hydrology 352(3-4): 379-387.

De Roo, A. P. J., C. G. Wesseling, et al. (1994). LISEM: a new physically-based hydrological and soil erosion model in a GIS-environment, theory and implementation. IAHS publication.(224): 439.

Eijkelkamp (2008). Operating Instructions 09.02 Laboratory Permeameters. The Netherlands: pp 15.

Eijkelkamp (2009a). Operating Instructions 09.04 Double Ring Infiltrometer Set. The Nertherlands: pp 9.

Eijkelkamp (2009b). Operating Instructions: 07 Sample Ring Kits. . The Netherlands: pp 12.

Eisenbies, M. H., W. M. Aust, et al. (2007). Forest operations, extreme flooding events, and considerations for hydrologic modeling in the Appalachians--A review. Forest Ecology and Management 242(2-3): 77-98.

FEMA (2000). Guidelines for Determining Flood Hazards on Alluvial Fans. Washington, D.C., United States Federal Emergency Management Agency (FEMA).

Hamilton, D. L., L. Simons, et al. (1988). Analysis of flows on alluvial fans : state of the Art. Phoenix, AZ, Arizona Dept. of Transportation. United States. Federal Highway Administration.

Heritage, G. L., D. J. Milan, et al. (2009). Influence of survey strategy and interpolation model on DEM quality. Geomorphology 112(3-4): 334-344.

Hodgson, M. E., J. R. Jensen, et al. (2003). An evaluation of LIDAR- and IFSAR-derived digital elevation models in leaf-on conditions with USGS Level 1 and Level 2 DEMs. REMOTE SENSING OF ENVIRONMENT -NEW YORK- 84(2): 295-308.

Horritt, M. S. and P. D. Bates (2001). Effects of spatial resolution on a raster based model of flood flow. Journal of Hydrology 253(1-4): 239-249.

Howes, D. A., A. D. Abrahams, et al. (2006). One- and two-dimensional modelling of overland flow in semiarid shrubland, Jornada basin, New Mexico. Hydrological Processes 20(5): 1027-1046.

Hunter, G. J. and M. F. Goodchild (1994). Design and Application of a Methodology for Reporting Uncertainty in Spatial Databases. URISA 1994 Annual Conference Proceedings. Washington, D.C. USA, Urban and Regional Information Systems Association: 1:771-785. .

Hunter, G. J. and M. F. Goodchild (1997). Modeling the uncertainty of slope and aspect estimates derived from spatial database Geographical Analysis 29(1): 35-49.

Hunter, N. M., P. D. Bates, et al. (2007). Simple spatially-distributed models for mredicting flood inundation: A review. Geomorphology 90(3-4): 208-225.

Jetten, V. (2002). LISEM user manual. The Netherlands, Utrecht Centre for Environment and Landscape Dynamics, Utrecht University,.

Kuchment, L. S. (1997). Estimating the risk of rainfall and snowmelt disastrous floods using physically-based models of river runoff generation. IAHS PUBLICATION(239): 95-100.

Laguzzi, M. M., G. S. Stelling, et al. (2001). A Fully Coupled 1D & 2D System Specially Suited for Flooding Simulation. Proceedings of the Congress- International Association for Hydraulic Research C(Conf 29): 36-40.

Lhuyd, E. (1708). Review: A Letter from Mr. Edward Lhuyd, Keeper of the Ashmolean Museum in Oxford, to Dr. R.R. in Yorkshire; Giving an Account of a Book. Philosophical Transactions (1683-1775) 26: 143-167.

Lin, G.-F. and L.-H. Chen (2004). A non-linear rainfall-runoff model using radial basis function network. Journal of Hydrology 289(1-4): 1-8.

Lin, G.-F. and C.-M. Wang (2007). A nonlinear rainfall-runoff model embedded with an automated calibration method - Part 1: The model. Journal of Hydrology 341(3-4): 186-195.

Malet, J. P., A. V. Auzet, et al. (2003). Soil surface characteristics influence on infiltration in black marls: application to the Super-Sauze earthflow (southern Alps, France). Earth Surface Processes and Landforms 28(5): 547-564.

McCalla, G. R. I., W. H. Blackburn, et al. (1984). Effects of Livestock Grazing on Infiltration Rates, Edwards Plateau of Texas. Journal of Range Management 37(3): 265-269.

Mishra, K. S. and V. P. Singh (2004). Long-term hydrological simulation based on the Soil Conservation Service curve number. Hydrological Processes 18(7): 1291-1313.

Mishra, S. K., K. Geetha, et al. (2005). Long-term hydrologic simulation using storage and source area concepts. Hydrological Processes 19(14): 2845-2861.

Moradkhani, H. and S. Sorooshian (2008). General Review of Rainfall-Runoff Modeling: Model Calibration, Data Assimilation, and Uncertainty Analysis. Hydrological Modelling and the Water Cycle**:** 1-24.

NRC (National Research Council). (1996). Alluvial Fan Flooding. Washington, D.C., National Academy Press.

Oksanen, J. and T. Sarjakoski (2005). Error propagation of DEM-based surface derivatives. Computers & Geosciences 31(8): 1015-1027.

OMIV-EOST. (2009). Barcelonnette area, Torrential Activity. Services des Observatoires des Instabilites de Versants. Retrieved 04 August 2009, 2009, from http://eost.u-strasbg.fr/omiv/barcelo_area_torrential_hazard.html.

Parlange, J. Y. and G. Sander (1985). A simplified hydrological rainfall-runoff model -- Comment. Journal of Hydrology 80(3-4): 395-397.

Remaitre, A. (2006). Morphologie et dynamique des laves torrentielles : Applications aux torrents des Terres Noires du bassin de Barcelonnette (Alpes du Sud). Géographie physique, humaine, économique et régionale, l'UNIVERSITE de CAEN. PhD (selected portions translated using Google Translator).

Remaitre, A. (2009). Characteristics of Faucon: Assorted data and Information from previous and current research (discussions and materials).

Remaitre, A. and J.-P. Malet (2009). The effectiveness of check dams in controlling upstream channel stability. Check dams, morphological adjustments, and erosion control in torrential streams. C. Consesa-Garcia and M. A. Lenzi. Hauppauge, N.Y., Nova Science.

Remaitre, A., J. P. Malet, et al. (2005). Morphology and Sedimentology of a Complex Debris Flow in a Clay-shale Basin. Earth surface processes and landforms : the journal of the British Geomorphological Research Group. 30(3): 339-348.

Remaitre, A., J. P. Malet, et al. (2008). Influence of check dams on debris-flow run-out intensity. Nat. Hazards Earth Syst. Sci. Natural Hazards and Earth System Science 8(6): 1403-1416.

Rykiel Jr, E. J. (1996). Testing ecological models: The meaning of validation. Ecological modelling. 90(3): 229.

Sanjari, G., H. Ghadiri, et al. (2006). Grazing management and its effects on groundcover and runoff control in Queensland, Australia.

SARL, E. T. R. M. (2003). Étude hydraulique de torrent de Faucon. V. Koulinski. France, (Translated using Google Translator): 46.

Schmitz, O., D. Karssenberg, et al. (2009). Linking external components to a spatio-temporal modelling framework: Coupling MODFLOW and PCRaster. Environmental Modelling & Software 24(9): 1088-1099.

Schumm, S. A., M. P. Mosley, et al. (1987). Experimental fluvial geomorphology. New York, Wiley.

Singh, V. (2002). Is Hydrology Kinematic? Hydrological processes. 16: 667-716.

Sivakumar, B. (2008). Dominant processes concept, model simplification and classification framework in catchment hydrology. Stochastic Environmental Research and Risk Assessment 22(6): 737-748.

Smith, K. and R. Ward (1998). Floods : physical processes and human impacts. Chichester etc., Wiley & Sons.

Svetlitchnyi, A. A., S. V. Plotnitskiy, et al. (2003). Spatial distribution of soil moisture content within catchments and its modelling on the basis of topographic data. Journal of Hydrology 277(1-2): 50-60.

Tyagi, J. V., S. K. Mishra, et al. (2008). SCS-CN based time-distributed sediment yield model. Journal of hydrology. 352(3): 388.

Van Asch, T. W. J. and J. T. Buma (1997). Modelling Groundwater Fluctuations and the Frequency of Movement of a Landslide in the Terres Noires Region of Barcellonnette (France). Earth Surface Processes and Landforms 22(2): 131-141.

Weaver, W. E. (1986). Experimental study of alluvial fans. Colorado State University. Fort Collins. Colorado. Ph.D: 423 pp.

Weber, D. (1994). Research into earth movements in the Barcelonnette basin. Temporal occurence and forecasting of landslides in the European Community, Final report, Volume I. R. Casale, R. Fantechi and J. C. Flageollet, European Comission. **I:** pp 321-326.

Wieczorek, G. F., M. C. Larsen, et al. (2001). Debris-flow and Flooding Hazards Associated with the December 1999 Storm in Coastal Venezuela and Strategies for Mitigation, U.S. Geological Survey.

Wise, S. M. (2007). Effect of differing DEM creation methods on the results from a hydrological model. Computers & Geosciences 33(10): 1351-1365.

Wu, L., L. Pan, et al. (1999). Measuring Saturated Hydraulic Conductivity using a Generalized Solution for Single-Ring Infiltrometers. Soil Sci Soc Am J 63(4): 788-792.

Wu, S., J. Li, et al. (2008). A study on DEM-derived primary topographic attributes for hydrologic applications: Sensitivity to elevation data resolution. Applied Geography 28(3): 210-223.

Yamakoshi, T. (2004). History of RTM (Restauration des Terrains en Montagne) Projects in France. International Sabo Association. Retrieved January 04, 2010, from http://www.sabo-int.org/projects/france.html.

Zerger, A., D. I. Smith, et al. (2002). Riding the storm: a comparison of uncertainty modelling techniques for storm surge risk management. Applied Geography 22(3): 307-330.

Zhou, Q. and X. Liu (2004). Analysis of errors of derived slope and aspect related to DEM data properties. Computers & Geosciences 30(4): 369-378.

Appendix I

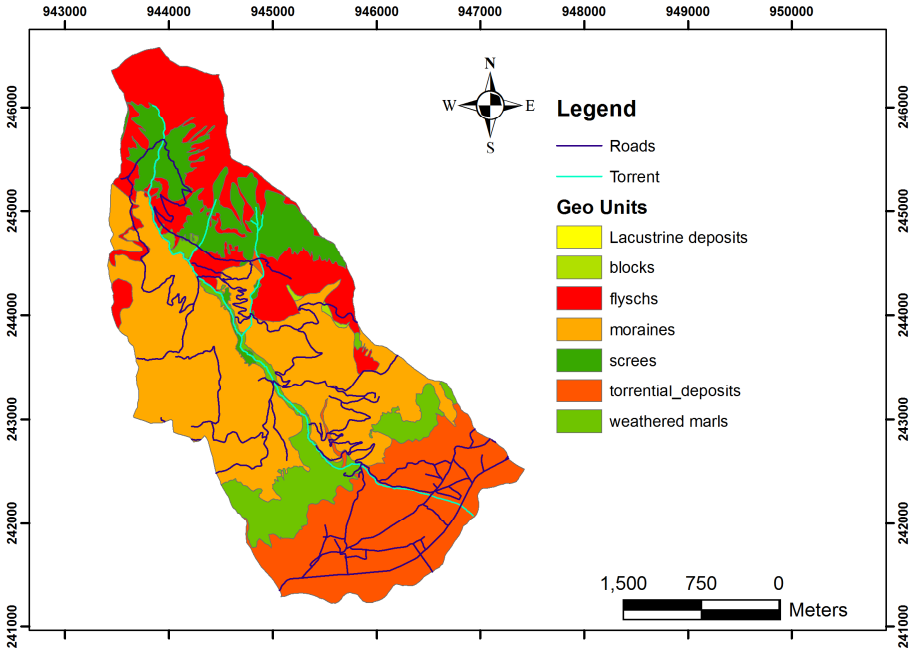

Appendix Figures 1 Soils/Morphology Types

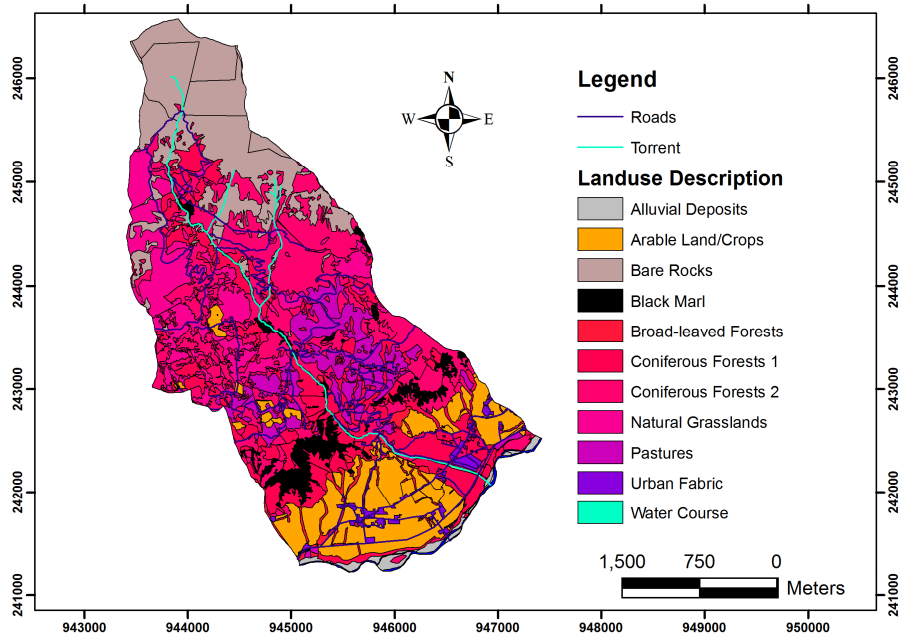

Appendix Figures 2 Landcover

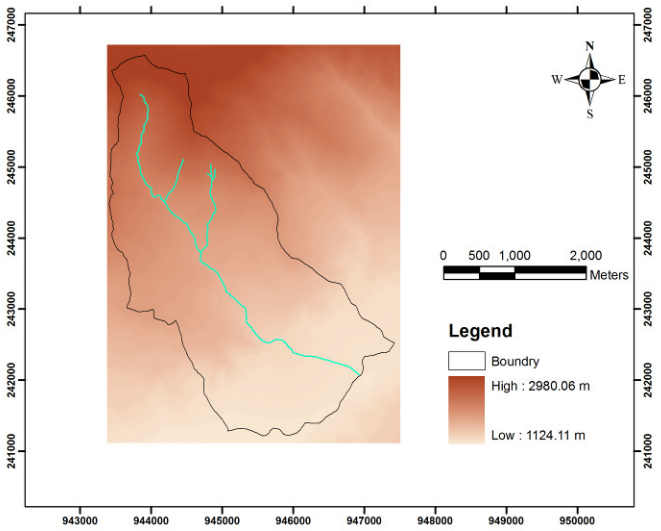

Appendix Figures 3 DTM

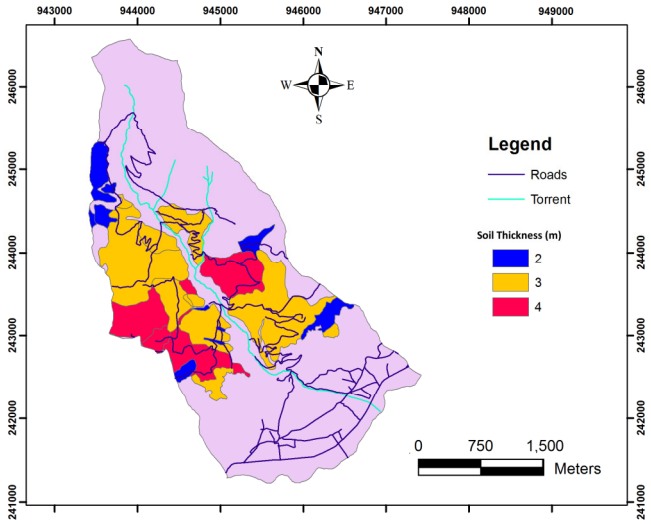

Appendix Figures 4 Soil Thickness

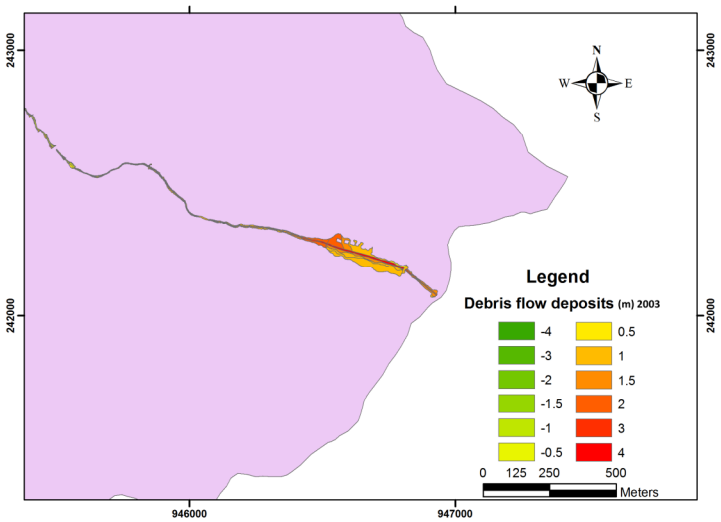

Appendix Figures 5 2003 Debris Deposits on the Alluvial Fan

Rain fall evaluation

These plots were created using the Extremes Toolkit in R-Statistics. The daily rainfall for Barcelonnette during the period June to October were plotted using a Generalized Pareto Distribution (GPD). The return period for various events is also displayed below. Also included is the SARL evaluation using the Gumbel method.

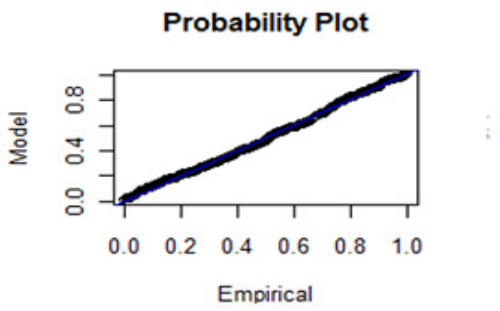

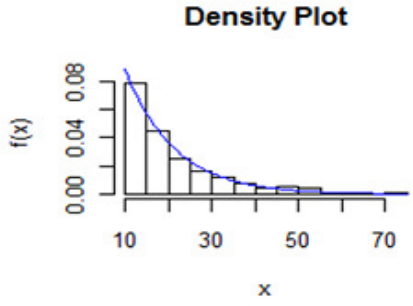

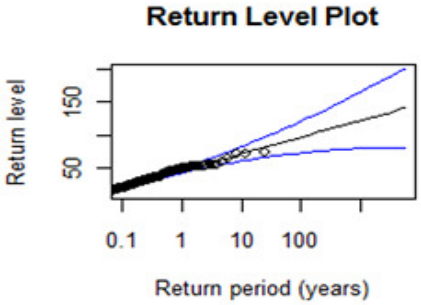

Return Period (yr)	Precipitation (mm)	95% conifence Limits	
1	46	43	50
5	64	57	74
10	71	63	83
20	79	68	92
50	89	75	104
100	97	81	113
500	114	95	134

Appendix Figure 7 Pareto Distribution of Barcelonnette Rainfall

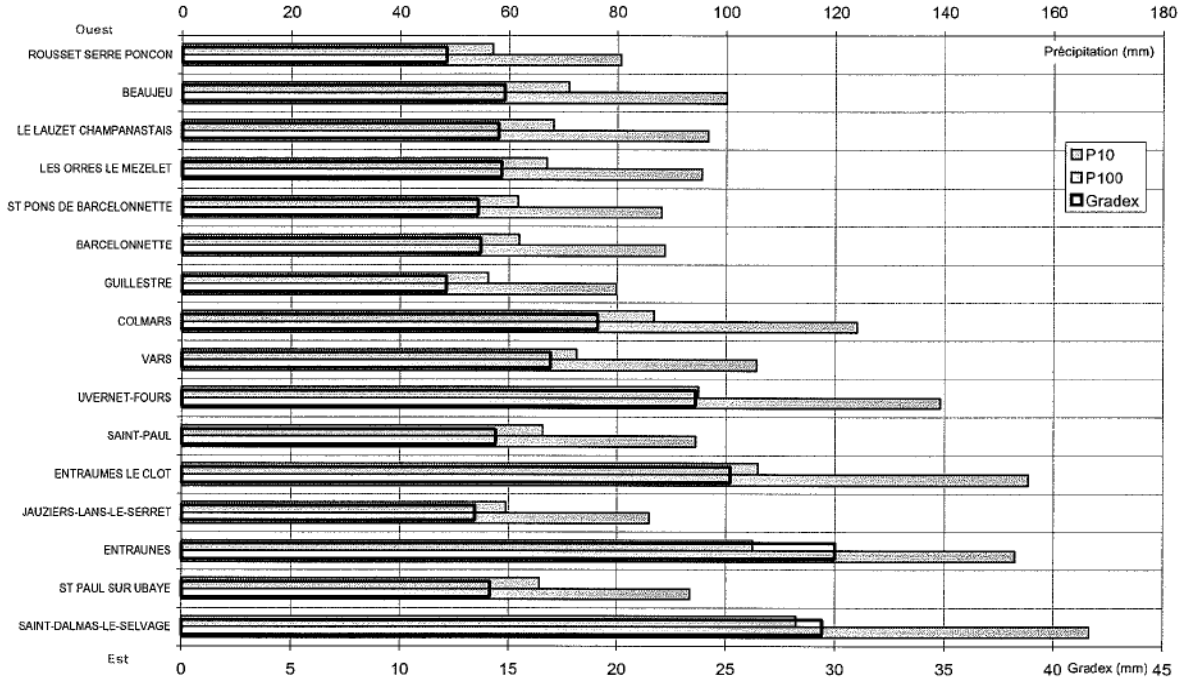

Appendix Figure 7 SARL (2003) evaluation of rainfall distribution of watersheds around Faucon

Appendix II

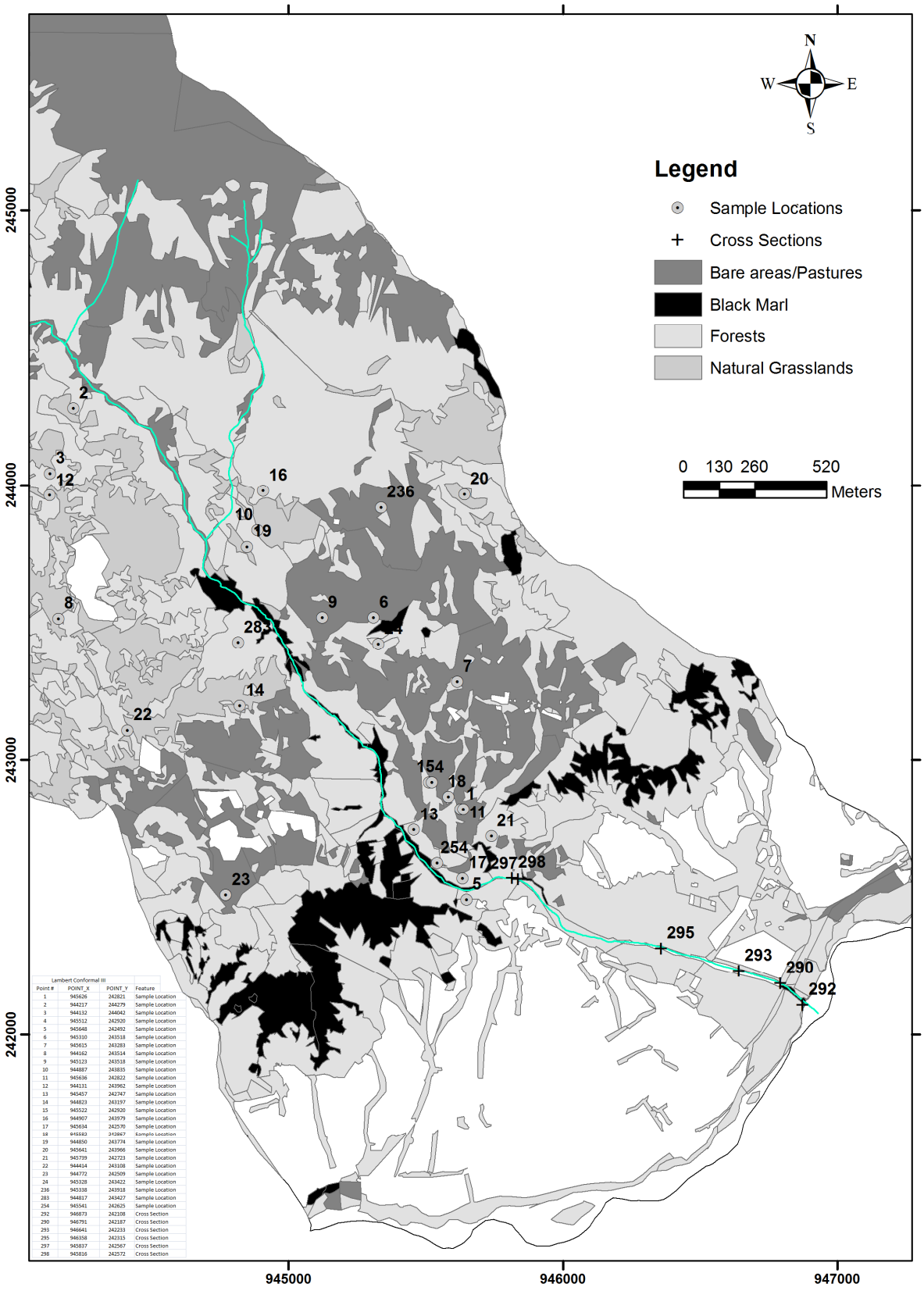

Point #	POINT_X	POINT_Y	Feature
1	945626	242821	Sample Location
2	944217	244279	Sample Location
3	944132	244042	Sample Location
4	945512	242920	Sample Location
5	945648	242492	Sample Location
6	945310	243518	Sample Location
7	945615	243283	Sample Location
8	944162	243514	Sample Location
9	945123	243518	Sample Location
10	944887	243835	Sample Location
11	945636	242822	Sample Location
12	944131	243962	Sample Location
13	945457	242747	Sample Location
14	944823	243197	Sample Location
15	945522	242920	Sample Location
16	944907	243979	Sample Location
17	945634	242570	Sample Location
18	945583	242847	Sample Location
19	944850	243774	Sample Location
20	945641	243966	Sample Location
21	945739	242723	Sample Location
22	944414	243108	Sample Location
23	944772	242509	Sample Location
24	945328	243422	Sample Location
236	945338	243918	Sample Location
283	944817	243427	Sample Location
254	945541	242625	Sample Location
292	946873	242108	Cross Section
290	946791	242187	Cross Section
293	946641	242233	Cross Section
295	946358	242315	Cross Section
297	945837	242567	Cross Section
298	945816	242572	Cross Section

Appendix Table 1 Summary of field observations

Ring #	Coordinates UTM, WGS84 X	Y	Ksat Pseudo Lab mm/hr	P-meter mm/hr	Field mm/hr	Ring Size	Soil Type	Porosity %	Bulk Density g/cm^3	Initial soil moisture %	colour wet	gravel %	Top Soil layer cm	Remarks about pF sample post inspection
1	315120.0	4919300.0	28.7		34.0	Large	Sandy Clay Loam	50.1	1.5		7.5 yr 5/1	10.0	3	1.5 cm gravel, regolith, pore spaces
2	313833.0	4920867.0	286.6	387.9			Fine sandy clay	60.3	0.9	0.5	10 yr 3/1	50.0	5	2 cm humas, regolith,
3	313729.0	4920638.0	1579.0	13077.5			Fine sandy clay	51.6	1.1	0.5	5 yr 5/1	40.0	30	pore spaces, regolith, 4mm gravel
4	315014.0	4919407.0	188.1		53.8	Small	Fine sandy clay	51.9	1.2		7.5 yr 5/1	20.0	10	long root, 1 cm gravel, regolith
5	315115.0	4918970.0	335.8	13.0	365.2	Large	Clay	59.3	1.1	0.6	10 yr 3/1	5.0	20	3mm humas,layered with spaces
6	314861.0	4920020.0		310.0			Fine sandy clay	56.4	1.1	0.2	10yr 5/1	15.0		1cm gravel, pores, cracks
7	315146.0	4919761.0		9.4			Sandy Clay/Clay	59.3	1.0	0.3	10 yr 4/1	2.0	10	layered with spaces
8	313717.0	4920109.0		47.4			Sandy loam	46.4	1.3	0.3	10 yr 4/1	2.0		b. root, layered, pores
9	314675.0	4920035.0	37.2	12.1	62.7	Large	Fine sandy clay	49.4	1.4		10yr 5/1	7.0	5	4 cm root 2 cm gravel
10	314465.0	4920370.0	367.8	166.0	121.0	Small	Sandy Clay Loam	65.1	0.8		10 yr 3/1	40.0	10	humas, mixed with s. gravel
11	315130.0	4919300.0	39.9	6.0	17.1	Small	Sandy Clay Loam	47.8	1.3		7.5 yr 5/1	7.0	3	spaces, regolith
12	313722.0	4920558.0	268.7	884.2			Clay	61.8	0.9	0.5	5 yr 4/1	5.0	15	regolith, fine material, pores,
13	314945.0	4919239.0		1890.8	80.1	Small	Sandy Clay	48.8	1.0	0.4	10 yr 4/1	15.0		regolith, fine material, pores, roots,
14	314350.0	4919739.0		319.7	66.2	Small	Sandy Clay	69.7	1.0	0.4	7.5 yr 4/1	10.0		roots in 1cm
15	315024.0	4919407.0	133.6	51.2			Fine sandy clay	51.7	1.2		10 yr 4/1	30.0	10	3mm humas,
16	314497.0	4920512.0		548.5	86.7	Small	Sandy Clay	48.9	1.1	0.2	10 yr 5/1	10.0		mixed humas,pores on edge
17	315107.0	4919049.0	186.7	130.6	297.3	Large	Fine sandy clay	53.8	1.1		10 yr 4/1	20.0	10	mixed humas,pores
18	315080.0	4919349.0	519.1		196.1	Large	Sandy Clay Loam	50.8	1.3		10 yr 5/1	50.0	2	layered with spaces
19	314423.0	4920312.0	141.6	162.9			Sandy Clay	63.7	0.6		10 yr 4/1	5.0		1 cm humas, regolith
20	315227.0	4920440.0	2777.7	502.3	597.4	Large	Fine sandy clay	59.5	0.9	0.5	5 yr 4/1	2.0	8	5cm roots, pores, humas,
21	315224.0	4919193.0	190.8		44.0	Small	Sandy Clay	50.7	1.1		7.5 yr 3/1	30.0		sandy, humas,regolith,
22	313935.0	4919684.0		148.7	36.2	Small	Sandy Clay	58.4	1.0	0.5	7.5 yr 4/1	30.0	15	sandy, h. root density,regolith,
23	314243.0	4919058.0		1033.0	8.0	Small	Sandy Clay/Clay	38.3	1.9	0.2	10 yr 6/1	50.0		b. spaces, regolith
24	314871.0	4919923.0		17.0	72.0	Small	Sandy Clay	41.4	1.5	0.3	7.5 yr 6/1	7.0		b. spaces, regolith
236	314921.0	4920416.0			37.3	Large	Fine sandy clay							
283	314362.0	4919969.0			36.5	Small				0.4				
254	315019.0	4919111.0			82.8	Large	Clay							

Appendix III

```
//Program to generate random matrix and
added to DTM
fo = mopen("sdu.txt", "r");//dtm
fo1 = mopen ("sdsm.txt","r");// defined dsm
features with fixed elevation, such as
buildings, dikes, debris...
fp = mopen("new_topodsm.asc", "w"); //new
dsm
sc = 1; //sc = 1 means spatial correlated;
sc = 0 means random added
scal_fac = 0.002; //scale factor
[num_read,head1] =  mfscanf(fo, "%s");
[num_read,cool] =  mfscanf(fo, "%i");
[num_read1,head11] =  mfscanf(fo1, "%s");
[num_read1,cool1] =  mfscanf(fo1, "%i");
mfprintf(fp, "%s %i \n",head1,cool) ;
[num_read,head2] =  mfscanf(fo, "%s");
[num_read,roow] =  mfscanf(fo, "%i");
[num_read,head21] =  mfscanf(fo1, "%s");
[num_read,roow1] =  mfscanf(fo1, "%i");
mfprintf(fp, "%s %i \n",head2,roow) ;
[num_read,head3] =  mfscanf(fo, "%s");
[num_read,headx] =  mfscanf(fo, "%f");
[num_read1,head31] =  mfscanf(fo1, "%s");
[num_read1,headx1] =  mfscanf(fo1, "%f");
mfprintf(fp, "%s %.2f \n",head3,headx) ;
[num_read,head4] =  mfscanf(fo, "%s");
[num_read,heady] =  mfscanf(fo, "%f");
[num_read1,head41] =  mfscanf(fo1, "%s");
[num_read1,heady1] =  mfscanf(fo1, "%f");
mfprintf(fp, "%s %.2f \n",head4,heady) ;
[num_read,head5] =  mfscanf(fo, "%s");
[num_read,headSIZE] =  mfscanf(fo, "%f");
[num_read1,head51] =  mfscanf(fo1, "%s");
[num_read1,headSIZE1] =  mfscanf(fo1,
"%f");

mfprintf(fp, "%s %.2f \n",head5,headSIZE) ;
[num_read,head6] =  mfscanf(fo, "%s");
[num_read,headNO] =  mfscanf(fo, "%f");
[num_read1,head61] =  mfscanf(fo1, "%s");
[num_read1,headNO1] =  mfscanf(fo1, "%f");
  headNO1 = -999.00;

mfprintf(fp, "%s %.2f \n",head6,headNO1);

//random generate K of asc size normal dis.
mean X  sd x 'nor',X,x ;
N_ran = grand(roow,cool,'nor',0,0.5);

i = 1;
j = 1;
while (i <= roow);
  j = 1;
  while (j <= cool);
    [num_read,valoes] = mfscanf(fo, "%f");
    [num_read1,valoes1] = mfscanf(fo1,
"%f");
    v(i,j) = valoes;
    v1(i,j) = valoes1;
    j = j + 1;
  end;
  i = i + 1;
 end;

 //compute spatial autocorrelate random
values
 // v is our matrix, N_ran is our random
matrix
 //W is a weight matrix of 0 in non-acffect
areas
 // rand_V = iterate [ scale_fact * W * v]+
N_ran
 v11 = ones(roow,roow);
 rand_V = v;
 SD1 = 0.0;
 SD2 = 100000.0;
 SD_D = abs((SD2-SD1)/SD2);
 while (SD_D > 0.1);
   SD1 = SD2;
   if sc==1 then
   rand_V = scalfac * v11 * rand_V + N_ran;
   else
   rand_V = N_ran;
   end
   SD2 = stdev(rand_V);
   SD_D = abs((SD2-SD1)/SD2);
    mprintf('%f standard deviation \n',SD2)
 end

//  vv = v + rand_V;

i = 1;
j = 1;
while (i <= roow);
  j = 1;
  while (j <= cool);

    if (v1(i,j)> 0) then
    vv(i,j) = v1(i,j);
    else
    vv(i,j) = v(i,j) + rand_V(i,j);
    end

    r = vv(i,j);

    if (j == cool) ;
      mfprintf(fp, "%.2f \n",r);
    else  mfprintf(fp, "%.2f ",r);
    end;
    j = j + 1;
  end;
  i = i + 1;
 end;
 mclose (fo);
 mclose(fo1);
mclose (fp);
//mprintf('/f',SD_D);
mprintf("program complete")
```

```
// Program to analyize time series of matrix A & B and computer
time series of A * B per element = timeseries C
// Program also computes Max C value per in timeseries to give
static map of Value C


//parameters;
//# of files to read (input1.asc...input100.asc) => 100 (user
prompt) nflies value;
//Name of input file A time series (depth1.asc...depth100.asc) =>
depth change infile1 name;
//Name of input file B time series (velocity1.asc...velocity.asc) =>
velocity change infile2 name;
//Type of extension (input1.asc...input100.asc) => asc change
exten name;
// Temp file for writing information into => tempinfile.txt change tf
name [can be left as is];
// Name of timeseries C, without extension and numbering =>
impulse change Oputs name;
// Name of Static C, without extension and numbering => impulse
change Oput name;
// Number of significant zeroes in file name ex. input0001.asc => 3
change ceroeX name;

nfiles = input("How many files?");
infile1 = "dm1c"; //velocity
infile2 = "dm1d"; //depth
outfile1 ="impulse"
extn = "asc";
tf = "tempinfile.txt";
OputD = "Max_D.asc";
OputV = "Max_V.asc";
OputI = "Max_I.asc";
ceroeX = 3;
MAX_limit = 500;
OD = zeros(MAX_limit,MAX_limit);
OV = zeros(MAX_limit,MAX_limit);
OI = zeros(MAX_limit,MAX_limit);

// initalize values;
i = 0;
runnum = 1;
hed99 = -999;



//writes file names for T-Series;
ftp = mopen(tf,"w");
for i = 0:nfiles;
 if i < 10 then
   ceroes = ceroeX;
 elseif i < 100 then
   ceroes = ceroeX - 1;
 elseif i < 1000 then
   ceroes = ceroeX - 2;
 elseif i < 10000 then
   ceroes = ceroeX - 3;
 else ceroes = ceroeX - 4;
 end

 if ceroes == 1 then
  Z = "0" ;
 elseif ceroes == 2 then
  Z = "00" ;
 elseif ceroes == 3 then
  Z = "000" ;
 elseif ceroes == 4 then
  Z = "0000" ;
 else Z = "00000";
 end
  mfprintf(ftp, "%s%s%i.%s %s%s%i.%s %s%s%i.%s
\n",infile1,Z,i,extn,infile2,Z,i,extn,outfile1,Z,i,extn) ;
end;
mclose(ftp);

ftp = mopen(tf,"r");

finread = 0;
[numread,S1,S2,S3] = mfscanf (ftp, "%s %s %s");

while (finread ==0)


fo1 = mopen(S1, "r");
fo2 = mopen(S2, "r");
fo3 = mopen(S3, "w");

//read header = Assumes head is the same
[num_read1,g1,g2,g3,g4,g5,g6,g7,g8,g9]=mfscanf(fo1, "%s %s
%s %s %s %s %s %s");
[num_read1,g10,g11,g12,g13,g14,g15]=mfscanf(fo1, "%s %s %s
%s %s %s");
[num_read1,head1] =  mfscanf(fo1, "%s");
[num_read1,cool] =  mfscanf(fo1, "%i");
[num_read1,head2] =  mfscanf(fo1, "%s");
[num_read1,roow] =  mfscanf(fo1, "%i");
[num_read1,head3] =  mfscanf(fo1, "%s");
[num_read1,headX] =  mfscanf(fo1, "%f");
[num_read1,head4] =  mfscanf(fo1, "%s");
[num_read1,headY] =  mfscanf(fo1, "%f");
[num_read1,head5] =  mfscanf(fo1, "%s");
[num_read1,headSIZE] =  mfscanf(fo1, "%f");
[num_read1,head6] =  mfscanf(fo1, "%s");
[num_read1,headNO] =  mfscanf(fo1, "%f");

[num_read2,g1,g2,g3,g4,g5,g6,g7,g8,g9]=mfscanf(fo2, "%s %s
%s %s %s %s %s %s");
[num_read2,g10,g11,g12,g13,g14,g15]=mfscanf(fo2, "%s %s %s
%s %s %s");
[num_read2,head1] =  mfscanf(fo2, "%s");
[num_read2,cool] =  mfscanf(fo2, "%i");
[num_read2,head2] =  mfscanf(fo2, "%s");
[num_read2,roow] =  mfscanf(fo2, "%i");
[num_read2,head3] =  mfscanf(fo2, "%s");
[num_read2,headX] =  mfscanf(fo2, "%f");
[num_read2,head4] =  mfscanf(fo2, "%s");
[num_read2,headY] =  mfscanf(fo2, "%f");
[num_read2,head5] =  mfscanf(fo2, "%s");
[num_read2,headSIZE] =  mfscanf(fo2, "%f");
[num_read2,head6] =  mfscanf(fo2, "%s");
[num_read2,headNO] =  mfscanf(fo2, "%f");


//writes impulse file = Assumes single file, not time series
```

```
mfprintf(fo3, "%s %i \n",head1,cool) ;
mfprintf(fo3, "%s %i \n",head2,roow) ;
mfprintf(fo3, "%s %.2f \n",head3,headX) ;
mfprintf(fo3, "%s %.2f \n",head4,headY) ;
mfprintf(fo3, "%s %.2f \n",head5,headSIZE) ;
mfprintf(fo3, "%s %.2f \n",head6,hed99);


i = 1;
j = 1;
 while (i <= roow);
  j = 1;
   while (j <= cool);
    [num_read1,valoes1] = mfscanf(fo1, "%f"); //reads velocity
    [num_read2,valoes2] = mfscanf(fo2, "%f"); //reads depths
//    computes impulse
       if (valoes1 < -900) then
        impul_val = hed99 ;
       elseif  (valoes2 < -900) then
        impul_val = hed99 ;
       else
       impul_val = valoes1 * valoes2;
      end
 // Allocates Maximum Depth, Velocity and Impulse
       if (valoes1 > OV(i,j))
        OV(i,j) = valoes1;
       end
       if (valoes2 > OD(i,j))
        OD(i,j) = valoes2;
       end
       if (impul_val > OI(i,j))
        OI(i,j) = impul_val;
       end
// Prints the impulse time series files
       if (j == cool) then
        mfprintf(fo3, "%.2f \n",impul_val);
       else
        mfprintf(fo3, "%.2f ",impul_val);
       end;
   j = j + 1;
   end;
   i = i + 1;
 end;
mclose (fo1);
mclose (fo2);
mclose (fo3);

//checks for end of file
 [numread,S1,S2,S3] = mfscanf (ftp, "%s %s %s");
    if (numread <= 0)
      finread = 1;
      printf ('%s %i \n', "end", runnum)
    else
      printf ('%s %i \n', "continue", runnum)
      runnum = 1 + runnum;
    end

end
```

```
//prints the maximum velocity, Depth and Impulse files
fo4 = mopen(OputV, "w");
fo5 = mopen(OputD, "w");
fo6 = mopen(OputI, "w");
mfprintf(fo4, "%s %i \n",head1,cool) ;
mfprintf(fo4, "%s %i \n",head2,roow) ;
mfprintf(fo4, "%s %.2f \n",head3,headX) ;
mfprintf(fo4, "%s %.2f \n",head4,headY) ;
mfprintf(fo4, "%s %.2f \n",head5,headSIZE) ;
mfprintf(fo4, "%s %.2f \n",head6,hed99);
mfprintf(fo5, "%s %i \n",head1,cool) ;
mfprintf(fo5, "%s %i \n",head2,roow) ;
mfprintf(fo5, "%s %.2f \n",head3,headX) ;
mfprintf(fo5, "%s %.2f \n",head4,headY) ;
mfprintf(fo5, "%s %.2f \n",head5,headSIZE) ;
mfprintf(fo5, "%s %.2f \n",head6,hed99);
mfprintf(fo6, "%s %i \n",head1,cool) ;
mfprintf(fo6, "%s %i \n",head2,roow) ;
mfprintf(fo6, "%s %.2f \n",head3,headX) ;
mfprintf(fo6, "%s %.2f \n",head4,headY) ;
mfprintf(fo6, "%s %.2f \n",head5,headSIZE) ;
mfprintf(fo6, "%s %.2f \n",head6,hed99);
i = 1;
j = 1;
for i=1:roow
  for j=1:cool
    if (j == cool) then
      mfprintf(fo4, "%.2f \n",OV(i,j));
      mfprintf(fo5, "%.2f \n",OD(i,j));
      mfprintf(fo6, "%.2f \n",OI(i,j));
      j =1;
      i = i+1;
      else
      mfprintf(fo4, "%.2f ",OV(i,j));
      mfprintf(fo5, "%.2f ",OD(i,j));
      mfprintf(fo6, "%.2f ",OI(i,j));
      j =1 + j;
     end;
    end
  end
  mclose(fo4);
  mclose(fo5);
  mclose(fo6);

mprintf("program complete")
```